Mathematical modeling of the eyespots in butterfly wings

Kang-Ling Liao[1,2,*] Wei-Chen Chang[3], Jeffrey M. Marcus[2], Jenn-Nan Wang[4]
1 Department of Mathematics, University of Manitoba, Manitoba, R3T 2N2, Canada
2 Department of Biological Sciences, University of Manitoba, Manitoba, R3T 2N2, Canada
3 Department of Mathematics, National Taiwan University, Taiwan, R.O.C.
4 Institute of Applied Mathematical Sciences, National Taiwan University, Taiwan, R.O.C.
∗ Corresponding author. E-mail address: Kang-Ling.Liao@umanitoba.ca

Abstract

Butterfly wing color patterns are a representative model system for studying biological pattern formation, due to their two-dimensional simple structural and high inter- and intra-specific variabilities. Moreover, butterfly color patterns have demonstrated roles in mate choice, thermoregulation, and predator avoidance via disruptive coloration, attack deflection, aposematism, mimicry, and masquerade. Because of the importance of color patterns to many aspects of butterfly biology and their apparent tractability for study, color patterns have been the subjects of many attempts to model their development. Early attempts focused on generalized mechanisms of pattern formation such as reaction-diffusion, diffusion gradient, lateral inhibition, and threshold responses, without reference to any specific gene products. As candidate genes with expression patterns that resembled incipient color patterns were identified, genetic regulatory networks were proposed for color pattern formation based on gene functions inferred from other insects with wings, such as *Drosophila*. Particularly detailed networks incorporating the gene products, Distal-less (Dll), Engrailed (En), Hedgehog (Hh), Cubitus interruptus (Ci), Transforming growth factor-β (TGF-β), and Wingless (Wg), have been proposed for butterfly border ocelli (eyespots) which helps the investigation of the formation of these patterns. Thus, in this work, we develop a mathematical model including the gene products En, Hh, Ci, TGF-β, and Wg to mimic and investigate the eyespot formation in butterflies. Our simulations show that the level of En has peaks in the inner and outer rings and the level of Ci has peaks in the inner and middle rings. The interactions among these peaks activate precursor cells of pigments to generate white, black, and yellow pigments in the inner, middle, and outer rings, respectively, which captures the eyespot pattern of wild type (*Bicyclus anynana*) butterflies. Additionally, our simulations suggest that lack of En generates a single black spot and lack of Hh or Ci generates a single white spot, and a deficiency of TGF-β or Wg will cause the loss of the outer yellow ring. These deficient patterns are similar to those observed in the eyespots of *Vanessa atalanta*, *Vanessa altissima*, and *Chlosyne nycteis*. Thus, our model also provides a hypothesis to explain the mechanism of generating the deficient patterns in these species.

Keyword: Butterfly wings, pattern formation, reaction-diffusion model, gene expression.

Introduction

Butterfly wing color patterns are an attractive model system for studying biological pattern formation. Color patterns are particularly suitable for such studies because they are structurally simple and two-dimensional, they consist of clearly defined subunits, and they are highly inter- and intra-specifically variable [1, 6, 14, 33, 39, 47]. Butterfly color patterns have demonstrated roles in mate choice [39, 59], thermoregulation [24], and predator avoidance (including camouflage [68], disruptive coloration [57], attack deflection [21], aposematism [15], mimicry [58], and masquerade [65]). Because of the importance of color patterns to many aspects of butterfly biology and their apparent tractability for study, color patterns have been the subjects of many attempts to model their development.

Each wing surface consists of a flat and static monolayer of epidermal cells [50]. A subset of the epidermal cells differentiate into scale cells [62, 64] which will synthesize pigments [26, 28] to generate

color patterns including border ocelli (also known as eyesopts) [50]. The number, location, and size of the eyespots differ among species of butterflies [50]. The position and shape of the wing color pattern are determined by the locations of signalling sources from the wing veins and wing margin [28, 47, 50]. Additionally, the pattern formation requires a two-step process: the determination of the distribution of discrete signalling sources for the color pattern during the last larval instar and the differentiation of the surrounding pattern during the pupal state [46]. The wing patterns (i.e., the background pattern or global pattern) are composed by five pattern elements: i) ripple patterns are the rhythmical patterns covering the whole wing surface, ii) dependent patterns are the pattern depended on the lacunae of the pupal wing, iii) crossbands are the band pattern alone the anterior to the posterior margin of the wing, iv) eyespots are the pattern consists of concentric rings with different colors, and the v) color fields are the large areas of the wing surface with color [44]. The position, number, size and color of eyespots are determined in a developmental pathway that is independent of other pattern elements and body structures [8]. The eyespot appears from an inductive organizing center, the focus, which is a signalling source of a morphogen to determine the pigment of surrounding cells [8]. The color of the wing patterns is determined by the pigment generated by scale cell surface features that reflect light [46, 61, 62, 64].

In [8], Brakefield et al. defined the developmental pathway for eyespot formation and then investigated how these pathways affect the numbers and sizes of eyespots in the squinting bush brown butterfly, *Bicyclus anynana* (Lepidoptera: Nymphalidae: Satyrinae). The experiments in *Bicyclus anynana* showed that the dynamics of the expression of *Distal-less (Dll)* gene can be used to categorize the eyespot formation into the following four stages [49]. Stage I - The larval prepattern: In the larva, a high level expression of Dll protein appears as a broad band and stripes down the middle of each wing subdivision to creates the potential focal pattern. Stage II - The focal determination: The Dll protein accumulates and is stabilized at the tips of these stripes and then diffuses to form stable circular spots of Dll expression. Stage III - The focal signaling: In the pupa, the high level of Dll expression expands to a broader circular region where the region is determined by the signaling from the epithelial focus. Stage IV - Differentiation: The positions of these spots of Dll expression become the central regions of the eyespots. Some graded morphogen appears across the radius of the eyespot region such that the surrounding cells of foci generate different pigmented scale types, according to the level or type of signal they receive and their location within the wing [8]. Based on this eyespot formation process, the Dll expression can be used to determine the position and number of foci and detect signaling from the focus [8]. Within the wing epidermis, the signalling molecules move through the extracellular medium by diffused through gap junctions [46]. Additionally, there is no cell migration within the wing epithelium, so the pattern is mainly affected by the cell differentiation in responsive to chemical signalling, instead of the cell movement [46, 50].

Many studies employ the activator-inhibitor type of models used by Turing [66] to investigate the wing pattern formation of butterfly [5, 13, 32, 43–45, 47, 48, 50, 61]. The first proposed model type is the gradient model that the morphogens produced by central cells of eyespots diffuse to the surrounding cells, and then the surrounding cells differentiate into discrete rings based on the received morphogen concentration [39, 44, 45, 47]. Nijhout provided gradient models based on the distribution information from focus of ocellus [44] to show that the foci are the sources of a diffusing chemical to activate color-specific biosynthetic pathways [45, 47] and to show that the chemical signal depending on cell position generates the surrounding patterns [47]. Nijhout also proposed a model involving the signaling from an activator in a lateral inhibition reaction to generate the required spatial distribution of sources and sinks such that the model can generate the eyespot patterns [46, 48]. Murray also proposed a diffusion model incorporating a diffusing morphogen resulting in the activation of a biochemical gene to generate the wing patterns in *lepidopteran* [43].

Bard et al. [5] provided a diffusion equation incorporating morphogen sources at the foci and sinks at the wing margin with appropriate diffusion throughout the wing. Since the morphogen concentration determines the pigments generated by scale cells, this model is able to generate wing patterns for different species of butterflies [5]. In [61], Sekimura et al. created a modified Turing mechanism reaction-diffusion

model, involving different regions in the wing and spatially dependent morphogen, to generate the global pattern on the wing of *P. dardanus* on a geometrically accurate wing domain. Sekimura et al. used this model to investigate the parameter values for mode selection, threshold values for color determination, wing shape and boundary conditions [61], and then predict the global effect on wing patterns in cutting experiments [32] which cannot be generated from the model mentioned in [47]. In [13], Dilao and Sainhas provided a reaction-diffusion model, involving two diffusive morphogens for the first eyespot ring formation and the modification of wing background pigment precursors, to generate the general structural organization of eyespots.

These activator-inhibitor models provide analysis of color pattern formation based on the interaction between generalized activator and inhibitor morphogens, but they still lack detailed information concerning the specific morphogens and signaling processes involved in the development of butterfly eyespots. Thus, based on the findings from activator-inhibitor models, researchers started to build models with detailed structural analysis of eyespots. In [52–54], Otaki provided a simple uniformly decelerated motion model describing the interaction between the morphogenic signals and parafocal elements (PFEs) to investigate the universally morphological feature inside-wide rule of eyespots: one eyespot contains one inner core black ring and an outer black ring. In [63], Sekimura et al. built a spatially two-dimensional reaction-diffusion system model with non-homogeneous Dirichlet boundary conditions to investigate the mechanism for determination of the number and location of eyespots. Their simulation results suggested that the morphogen concentration along the proximal vein is the main factor to control the distribution of eyespots and this observation is robust to the proximal boundary condition [63].

In [14], Evans and Marcus provided several reaction-diffusion models to generate the concentrations of gene expression during the eyespot formation in *Bicyclus anynana* and *Junonia coenia*. Comparing their simulation result with experimental data for these gene expressions, they made the following conjecture. In the eyespot foci (i.e., the inner ring of the eyespot), firstly, the expression of Notch gene induces the co-expression of Notch and Distal-less (Dll). Secondly, the expression of Dll activates the expression of the gene Engrailed (En). Thirdly, the expression of En shows positive associations with the expression patterns of hedgehog (Hh) transcript. Fourthly, the expression of hh triggers the expression of Patched (Ptc) and the transcription factor Cubitus interruptus (Ci), which suggested that the expression of hh promotes the expression of Ci. However, the hh expression inhibits the production of Ci within intracellular reaction suggesting that the intracellular function of hh actually suppresses the expression of Ci. In [34], Marcus and Evans used the model mentioned in [14] to generate the wing patterns in two mutants, the comet mutation with a series of comet-shaped eyespot foci and the Cyclops mutation with failure in wing vein formation. In [33], Marcus provided more complete information about the downstream pathways of En gene expression, such as how the interaction between the TGF-β signaling and Wingless (Wg) signaling affects the localization of eyespots. Additionally, Marcus also explained the mechanism for generating different pigments in different region within the eyespots: the concentration of En in the inner and outer rings is used to generate the white and yellow pigments in the inner and outer rings respectively, and the concentration of Ci is used to active the generation of black pigment in the middle region of the eyespots [33].

A summary of these mathematical models and the focus of this work are listed in the Table 1. In Table 1, all model types (i.e., the second column) incorporate cellular responses to diffusing morphogens. Models that incorporated generalized reaction-diffusion interactions are labeled as reaction-diffusion models. Gradient models incorporate a diffusion term that represents the gradient of a single activator, while Turing reaction-diffusion models include two morphogens: one activator and one inhibitor. Therefore, these models used different mathematical approaches and cannot be mutually replaced. We use the Wolpert Positional Information (PI) theory mentioned in [69, 70] to define different types of patterning mechanisms: In the fourth column, the de-novo patterning refers to the initial specification of developmental pre-patterns and organizers whereas the fine-scale patterning represents the effect of those pre-patterns and organizers on the surrounding cells and tissues.

Table 1. Summary of mathematical models for eyespot formation. The reference, type, and the stage defined in [8] of the models are listed in the first, second, and third columns, respectively. The patterning type defined in [69, 70] is shown in the fourth column. The fifth column shows whether the model incorporates molecular or genetic information. The last column describes whether the simulation results are only hypothetical or have support from experiments.

Model	Type	Stage	De-novo v.s. fine-scale patterning	Molecular & genetic details	Hypothesis v.s. experiment
Nijhout 1978 [44]	Gradient model	II	De-novo	Excluded	Experiment [16, 44]
Murray 1981 [43]	Turing reaction-diffusion model (inhibitor-activator)	II & III	De-novo/Fine-scale	Excluded	Experiment [43]
Bard & French 1984 [5]	Turing reaction-diffusion model (inhibitor-activator)	II & III	De-novo/Fine-scale	Excluded	Hypothesis
Nijhout 1980, Nijhout 1991 [45, 47]	Gradient model	II & III	De-novo	Excluded	Experiment [17, 45]
Nijhout 1990, Nijhout 1994 [46, 48]	Turing reaction-diffusion model (inhibitor-activator)	I &II	De-novo	Excluded	Experiment [63]
Sekimura et al 2000 [61]	Turing reaction-diffusion model (inhibitor-activator)	I	De-novo	Excluded	Experiment [32]
Dilaõ & Sainhas 2004 [13]	Turing reaction-diffusion model (inhibitor-activator)	IV	Fine-scale	Included	Experiment [17, 48]
Evans & Marcus 2006 [14]	Reaction-diffusion model	II	De-novo	Included	Experiment [14, 23, 27]
Marcus & Evans 2008 [34]	Reaction-diffusion model	II	De-novo	Included	Experiment [8]
Otaki 2011, Otaki 2012 [52–54]	Gradient model	IV	Fine-scale	Excluded	Experiment [54]
Sekimura et al 2015 [63]	Turing reaction-diffusion model (inhibitor-activator)	I & II	De-novo	Excluded	Experiment [63]
This work	Reaction-diffusion model	III	Fine-scale	Included	Hypothesis

In the current work, based on the interaction amount En, Hh, Ci, TGF-β, and Wg gene products in *Bicyclus anynana* and *Junonia coenia* mentioned in [14,33,34], we develop a system of partial differential equations (PDEs), including the concentrations of En, Hh, Ci, TGF-β, and Wg proteins, to mimic the eyespot formation in *Bicyclus anynana* butterflies. Our simulation shows that the concentration of En has one peak in the inner ring and one peak in the outer ring, as well as the concentration of Ci has one peak in the inner ring and one peak in the middle ring. High concentrations of En and Ci in the inner ring trigger cells to express the biosynthetic pathway responsible for making white pigment (pteridine) , high concentration of Ci in the middle ring activates ce;;s tp express the biosynthetic pathway responsible for making black pigment (dopa melanin), and the high concentration of En in the outer ring initiates expression of components of the biosynthetic pathway for the yellow pigment (pheomelanin). Therefore, our simulation captures the generation dynamics of white, black, and yellow pigments in the inner, middle, and outer rings respectively which fits the pattern of wild type *Bicyclus anynana* butterflies described in [33]. On the other hand, we use this model to predict the eyespot patterns in knockout mutants. Our simulations display three types of degenerated patterns: (i) a single black spot observed from *Vanessa atalanta* is caused by the deficiency of En; (ii) a single white spot observed from *Vanessa atalanta* and *Vanessa altissima* is caused by the deficiency of Hh or Ci; and (iii) loss of the outer yellow ring shown from *Chlosyne nysteis* is caused by the loss of TGF-β or Wg. A summary of our work for the eyespot patterns in wild type *Bicyclus anynana* butterflies and these null mutants is shown in Fig 1. Finally, our sensitivity analysis shows that (i) increasing the production rate of Ci in inner ring, or reducing the production rate of Hh in inner ring or the production rate of Ci in middle ring promotes the white pigment formation in the inner ring; (ii) enhancing the production rate of Ci in middle ring or degradation rate

of En, or reducing the production rates of En, Hh, or Ci in inner ring, or the diffusion rate of TGF-β promotes the black pigment formation in the middle ring; and (iii) increasing the production rate of En in outer or inner rings promotes the yellow pigment formation in the outer ring.

As listed in Table 1, most pervious mathematical models are based on the Turing reaction-diffusion model, and hence lack the molecular and genetic information and mainly capture the behavior in stage II during the eyespot pattern formation when the eyespot focus is specified. Thus, these models cannot be used to investigate how the gene expression results in eyespot ring formation in stages III and IV. Here we attempt to incorporate these missing stages in our model, so the main contribution of our work is to provide a different modeling approach incorporating molecular information to investigate how the cells react related to morphogens according to their distance from the focus in stage III.

Results

Mathematical model

Our mathematical model is based on the network described in Fig. 2. The variables that will be used are listed below. The values of parameters are listed in Table 2 and are estimated by using experimental data in the Method section:

$$\begin{aligned}
E(x,t) &= \text{concentration of En protein at location } x \text{ and time } t \text{ with unit } kD/cm,\\
H(x,t) &= \text{concentration of Hh protein at location } x \text{ and time } t \text{ with unit } kD/cm,\\
C(x,t) &= \text{concentration of Ci protein at location } x \text{ and time } t \text{ with unit } kD/cm,\\
T(x,t) &= \text{concentration of TGF-}\beta \text{ protein at location } x \text{ and time } t \text{ with unit } kD/cm,\\
W(x,t) &= \text{concentration of Wg protein at location } x \text{ and time } t \text{ with unit } kD/cm.
\end{aligned}$$

An eyespot consists of inner, middle, and outer rings. Thus, it is reasonable to consider the radially symmetric solutions and reduce the two dimensional spatial variable x to the one dimensional variable, r, representing the radius of the eyespot. The total eyespot area in wild type *Bicyclus anynana* is around 11.2 mm^2 [55] and the radius of the eyespot is around $R_0 = 0.094\ cm$. For simplicity, we focus on the eyespot region and nondimensionalize the distance between the center and boundary of the eyespot to be 1 by rescaling $R_0(= 0.094\ cm)$. In this work, we are mainly interested in the qualitative description of the eyespot patterns. Hence, we explicitly set the inner, middle, and outer rings as follows

$$\Omega_{in} := \{0 \le r \le 0.3\},\ \Omega_{mid} := \{0.3 \le r \le 0.6\},\ \Omega_{out} := \{0.6 \le r \le 1\}. \tag{1}$$

Next, we define the functions $\chi_{in}(r)$, $\chi_{mid}(r)$, and $\chi_{out}(r)$ as

$$\chi_{in}(r) = \frac{1}{1+e^{30(r-0.15)}}, \tag{2}$$

$$\chi_{mid}(r) = 1.5 \times \frac{1}{1+e^{-30(r-0.4)}} \times \frac{1}{1+e^{30(r-0.5)}}, \tag{3}$$

$$\chi_{out}(r) = \frac{1}{1+e^{-30(r-0.8)}}, \tag{4}$$

to restrict reactions in the inner, middle and outer rings, respectively. Notice that the simulation results for wild type and null mutants butterflies will not be changed, if the regions Ω_{in}, Ω_{mid}, and Ω_{out} are replaced by

$$\Omega_{in} := \{0 \le r \le a\},\ \Omega_{mid} := \{a \le r \le b\},\ \Omega_{out} := \{b \le r \le 1\},$$

with $0 < a < b < 1$ and the definitions of $\chi_{in}(r)$, $\chi_{mid}(r)$, and $\chi_{out}(r)$ are adjusted accordingly.

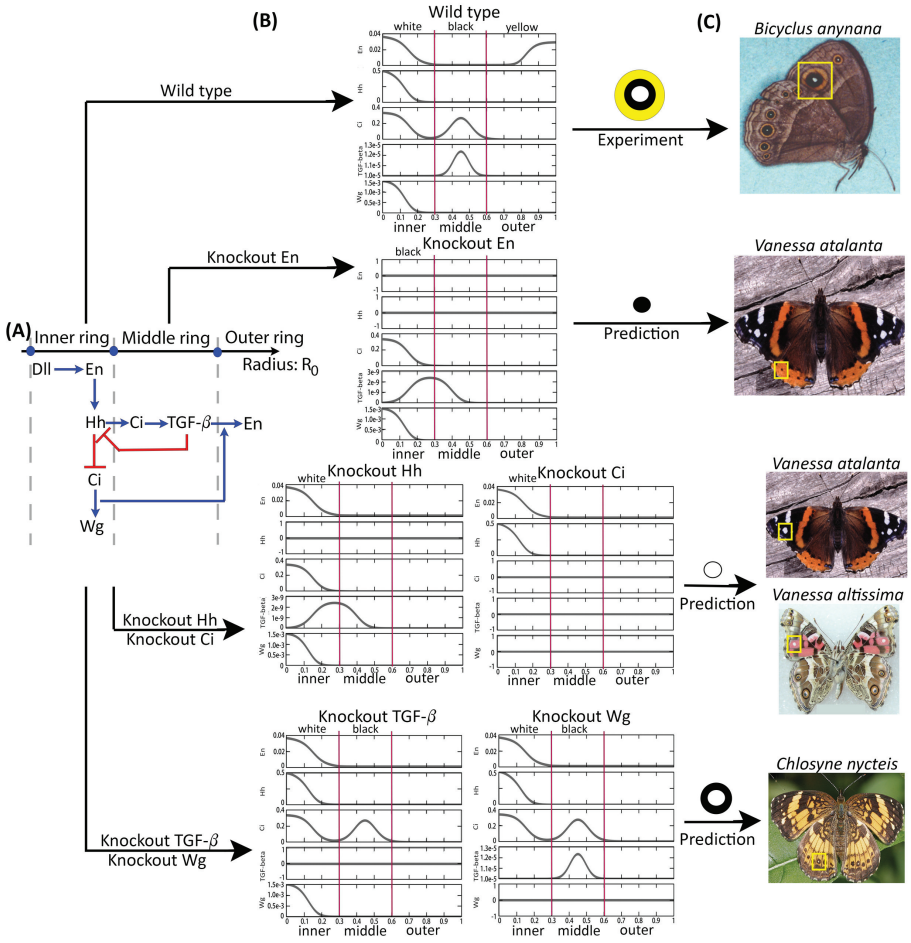

Figure 1. Summary of the relation between the system network and predicted eyespot pattern. (A) shows the system network among the five key gene expressions: En, Hh, Ci, TGF-β, and Wg of wild type *Bicyclus anynana*, based on experimental evidences. The detailed explanation of the network is shown in Fig. 2. (B) provides the gene expression profiles at 16 hours over the radius of the eyespot in wild type (the first row), En null mutant (the second row), Hh and Ci null mutants (the third row), and the TGF-β and Wg null mutants (the fourth row). The pink lines at radii 0.3 and 0.6 are used to separate the radius into inner ring between 0 and 0.3, middle ring between 0.3 and 0.6, and outer ring between 0.6 and 1. The expected pigment in the corresponding region is shown at the top of each region. (C) displays the species with the corresponding eyespot pattern marked in the yellow boxes. The first row shows the eyespot with white inner ring, black middle ring, and yellow outer ring in *Bicyclus anynana*. The second row provides the eyespot with black inner ring in *Vanessa ataianta*. The third row includes two cases for the white inner ring: one in *Vanessa atalanta* and the other in *Vanessa altissima*. The fourth row shows the white inner ring and black middle ring in *Chlosyne nycteis*. A cartoon eyespot pattern representing each phenotypic case is shown above each arrow between (B) and (C). The experiment and prediction listed below each arrow between (B) and (C) represent that the expected eyespot pattern is with and without experimental evidence, respectively.

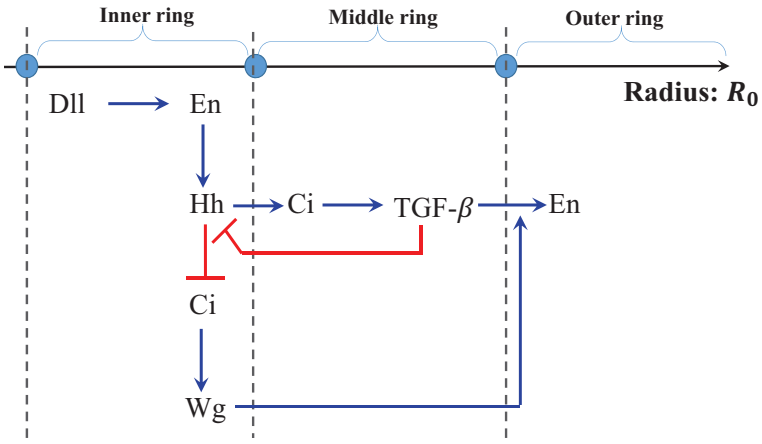

Figure 2. System network of the model. Initially, for the cells in the inner ring, the protein Dll triggers the gene expression of En to generate the mRNA and protein of En [40]. The generated En protein then triggers the gene expression of Hh [23], and then the produced Hh protein inhibits the gene expression of Ci in the inner ring [20, 67]. Next, the Hh protein diffuses to cell member to bind with the receptor patched on the cells in the middle ring to activate the phosphorylation of Ci protein in the middle ring [23]. In the middle ring, the phosphated Ci protein triggers the gene expression of TGF-β [23], and then the generated TGF-β protein diffuses to the outer ring to initiate the autoregulation of En protein [23]. Meanwhile, the TGF-β protein diffuses to the inner ring to inhibit the production of Hh protein [10] resulting in promoting Ci protein in the inner ring. Next, in the inner ring, the generated Ci protein binds with Wg protein to trigger the Wg signaling pathway [11]. The triggered Wg signaling pathway diffuses to the outer ring [55] to maintain the expression of En activated by the TGF-β [29, 51].

The equation for En protein (E)

The equation for the concentration of En protein is described by

$$\frac{\partial E}{\partial t} = \underbrace{\alpha_E \cdot \chi_{in}(r)}_{\text{source from Dll}} + \underbrace{(\lambda_E T \cdot \chi_{out}(r)) \cdot (W \cdot \chi_{out}(r))}_{\text{interaction between Wg and TGF-}\beta} - \underbrace{\mu_E E}_{\text{degradation}} . \tag{5}$$

The first term in the right-hand side of Eq. (5) represents a constant source of En protein from Dll in the inner ring [40]. The second term accounts for the autoregulation of En protein [23] maintained by the interaction between TGF-β protein and Wg protein in the outer ring [29, 51]. The last term is the degradation of En protein.

The equation for Hh protein (H)

The concentration of Hh protein satisfies the following equation

$$\frac{\partial H}{\partial t} = \underbrace{d_H \frac{1}{r^2}\frac{\partial}{\partial r}(r^2 \frac{\partial H}{\partial r})}_{\text{diffusion}} + \underbrace{(\alpha_H E \cdot \chi_{in}(r))}_{\text{promotion triggered by En}} \Big/ \underbrace{(1 + k_H T \cdot \chi_{in}(r))}_{\text{inhibition by TGF-}\beta} - \underbrace{\mu_H H}_{\text{degradation}} . \tag{6}$$

The first and last terms account for the diffusion and degradation of Hh protein. The second term shows that the Hh protein is triggered by En protein [23] and is inhibited by TGF-β protein [10] in the inner ring.

Table 2. Parameters of the whole model.

Parameter	Description	Value	Unit	Reference
d_H	diffusion rate of Hh	2.97017×10^{-7}	cm^2/min	[12] & Table 6
d_T	diffusion rate of TGF-β	3×10^{-7}	cm^2/min	[12] & Table 6
d_W	diffusion rate of Wg	2.91519×10^{-7}	cm^2/min	[12] & Table 6
μ_E	degradation rate of En	3.85082×10^{-4}	$/min$	[35] & Table 7
μ_H	degradation rate of Hh	1.38629×10^{-2}	$/min$	[18, 31, 56] & Table 6
μ_C	degradation rate of Ci	9.24196×10^{-3}	$/min$	[4] & Table 7
μ_T	degradation rate of TGF-β	5.77623×10^{-3}	$/min$	[60] & Table 6
μ_W	degradation rate of Wg	1.15525×10^{-3}	$/min$	[73] & Table 7
N_0	amount of Wg protein	1	kD/cm	estimated
R_0	radius of eyespot	0.094	cm	[55]
α_E	production rate of En in inner ring	$(3.56201 \times 10^{-2})N_0$	kD/cm	[55] & estimated
α_H	production rate of Hh in inner ring	2.18247×10^{-2}	$/min$	[55] & estimated
α_C	production rate of Ci in middle ring	1.20978×10^{-3}	$/min$	[55] & estimated
α_T	production rate of TGF-β in middle ring	1.89385×10^{-5}	$/min$	[55] & estimated
α_W	production rate of Wg in inner ring	9.46923×10^{-5}	$/min$	[55] & estimated
λ_E	production rate of En in outer ring	$\frac{3.56201 \times 10^{-2}}{N_0}$	$cm/kD/min$	[55] & estimated
λ_C	production rate of Ci in inner ring	$352.35N_0$	kD/cm	[55] & estimated
k_H	half-saturation of Hh	$1/(4N_0)$	cm/kD	estimated
k_C	half-saturation of Ci	$1/(932N_0)$	cm/kD	estimated

The equation for Ci protein (C)

The equation for the concentration of Ci protein is given by

$$\frac{\partial C}{\partial t} = \underbrace{\lambda_C}_{\text{production of Ci}} \cdot \underbrace{\frac{\chi_{in}(r)}{1+k_C H}}_{\text{inhibition by Hh in inner ring}} + \underbrace{\alpha_C}_{\text{production of Ci}} \cdot \underbrace{H \cdot \chi_{mid}(r)}_{\text{promotion by Hh in middle ring}} - \underbrace{\mu_C C}_{\text{degradation}} . \quad (7)$$

The first term represents the production of Ci protein inhibited by Hh protein in the inner ring [20, 67]. The second term shows the production of Ci protein trigged by Hh protein in the middle ring [23].

The equation for TGF-β protein (T)

We model the dynamics of TGF-β protein by the equation

$$\frac{\partial T}{\partial t} = \underbrace{d_T \frac{1}{r^2}\frac{\partial}{\partial r}(r^2 \frac{\partial T}{\partial r})}_{\text{diffusion}} + \underbrace{\alpha_T C \cdot \chi_{mid}(r)}_{\text{activation of TGF-}\beta\text{ in middle ring}} - \underbrace{\mu_T T}_{\text{degradation}} . \quad (8)$$

The first and the last terms account for the diffusion and degradation of TGF-β protein. The second term represents the activation of TGF-β protein by Ci protein in the middle ring [23].

The equation for Wg protein (W)

The concentration of Wg protein satisfies the following equation

$$\frac{\partial W}{\partial t} = \underbrace{d_W \frac{1}{r^2}\frac{\partial}{\partial r}(r^2 \frac{\partial W}{\partial r})}_{\text{diffusion}} + \underbrace{\alpha_W C \cdot \chi_{in}(r)}_{\text{activation by Ci}} - \underbrace{\mu_W W}_{\text{degradation}} . \quad (9)$$

The first and last terms account for the diffusion and degradation of Wg protein. The second term shows the activation of Wg protein by Ci protein in the inner ring [11].

The detailed molecular information to support Eqs. (5)-(9) comes from experimental data of insects with wings (mostly from *Drosophila*) [10, 11, 20, 23, 29, 40, 51, 67]. Since insects with wings, *Drosophila*, butterflies, and moths have a shared ancestor that also had wings [2], they share numerous similarities of wing structure and morphology, wing development, and molecular processes, including genetic architecture and mechanisms of gene regulation [2]. Thus, we transfer the molecular knowledge from well-studied insects with wings to butterflies to estimate the parameter values for butterflies and then use sensitivity analysis to study how these parameter values correlate to the eyespot pattern.

Initial condition (IC).

Initially, only En is presented in the inner ring due to the Dll gene expression. Therefore, we assume that En in the inner ring is a decreasing function with respect to the radius r with the maximum occurring at the center, i.e., $r = 0$, and En maintains the minimum in the middle and outer rings. The initial conditions for other variables are given based on their steady states shown in the Appendix. So we have

$$\begin{array}{lcl} E(r,0) & = & 185\times 10^{-5} + 10^{-2}\left(1-\dfrac{10}{3}r\right)\chi_{[0,0.3]}(r) \\ H(r,0) & = & 233\times 10^{-5} \\ C(r,0) & = & 61\times 10^{-5} \\ T(r,0) & = & 10^{-5} \\ W(r,0) & = & 10^{-5}, \end{array} \tag{10}$$

for $0 \le r \le 1$.

Boundary condition (BC) - Neumann BC.

All dependent variables are radially symmetric and have no flux at the boundary of the eyespot. In other words, we have

$$\frac{\partial \eta}{\partial r}(1,t) = 0 \tag{11}$$

for $\eta = \{E,\ H,\ C,\ T,\ W\}$ and $t \ge 0$. On the other hand, to guarantee that the solution is regular, i.e.,

$$\limsup_{r\to 0^+}\left|\frac{1}{r}\frac{\partial u}{\partial r}(r,t)\right| < \infty,$$

it is necessary that

$$\frac{\partial \eta}{\partial r}(0,t) = 0 \tag{12}$$

for $t \ge 0$.

Combining above equations, we obtain the following system of PDEs

$$\left\{\begin{array}{lcl} \dfrac{\partial E}{\partial t} & = & \alpha_E\cdot\chi_{in}(r) + (\lambda_E T\cdot\chi_{out}(r))\cdot(W\cdot\chi_{out}(r)) - \mu_E E \\ \dfrac{\partial H}{\partial t} & = & d_H\dfrac{1}{r^2}\dfrac{\partial}{\partial r}(r^2\dfrac{\partial H}{\partial r}) + (\alpha_H E\cdot\chi_{in}(r))/(1+k_H T\cdot\chi_{in}(r)) - \mu_H H \\ \dfrac{\partial C}{\partial t} & = & \dfrac{\lambda_C\chi_{in}(r)}{1+k_C H} + \alpha_C H\cdot\chi_{mid}(r) - \mu_C C \\ \dfrac{\partial T}{\partial t} & = & d_T\dfrac{1}{r^2}\dfrac{\partial}{\partial r}(r^2\dfrac{\partial T}{\partial r}) + \alpha_T C\cdot\chi_{mid}(r) - \mu_T T \\ \dfrac{\partial W}{\partial t} & = & d_W\dfrac{1}{r^2}\dfrac{\partial}{\partial r}(r^2\dfrac{\partial W}{\partial r}) + \alpha_W C\cdot\chi_{in}(r) - \mu_W W \end{array}\right. \tag{13}$$

with initial condition (10) and homogeneous Neumann boundary condition (11) and (12). For the model (13), as mentioned in Fig. 2, there are experimental data from insects with wings to support the qualitative interactions among the components [10, 11, 20, 23, 29, 40, 51, 67]. Thus, the assumptions of the model (13) are: (i) the symmetric shape of the eyespot, initial and boundary conditions, while all of these assumptions are close to the real situation; (ii) the similarity of the structure development and molecular processes between insects with wings and butterflies; and (iii) the estimated parameter values of k_H, k_C, μ_E, μ_H, and N_0. Notice that different value of N_0 affects the absolute values of α_E, λ_E, λ_C, k_H, and k_C, but the relative values amount these five values is fixed. Since the assumptions (ii) and (iii) affect the values of k_H, k_C, μ_E, μ_H, and N_0, we will perform sensitivity analysis to demonstrate that these five parameter values do not have significant effect on the model outcome. Thus, when the values of these five parameters in butterflies become available, the simulation outcome will not be changed or we will be able to predict the simulation outcome easily.

Numerical simulation

In this section, we use the model (13) with conditions (10), (11), (12) to simulate the patterns of eyespots in wild type (*Bicyclus anynana*) and null mutants of butterflies. We use the forward Euler method with time step $dt = 0.01$ minute and $dr = 0.001/R_0$ and run the program in MATLAB. We want to remark that due to (12) we drop the term $\frac{1}{r}\frac{\partial \eta}{\partial r}$ and take

$$\frac{1}{r^2}\frac{\partial}{\partial r}(r^2\frac{\partial \eta}{\partial r}) \approx \frac{\partial^2 \eta}{\partial r^2}$$

in our simulation. Since the dropped term is of lower order, the qualitative behaviors of the solutions will not be affected. In the following, the notations En, Hh, Ci, TGF-β, and Wg account for En, Hh, Ci, TGF-β, and Wg proteins, respectively.

Model validation by using the wild type

In this subsection, we first validate the mathematical model (13) by comparing the numerical simulation results with the patterns of eyespots in wild type species. Notice that the high concentration of En triggers the generation of white and yellow pigments in the inner and outer rings, respectively. A low concentration of En, the high concentration of Ci activates the production of black pigment. However, when both of En and Ci have high concentrations at the same location, the cells only generate white pigments. Additionally, since the Dll protein triggers the En expression in the inner ring, it takes around 16 hours to generate all pigments in the corresponding rings. To mimic the wild type eyespot pattern with white, black, and yellow pigments in the inner, middle, and outer rings, we expect that, at 16 hours, (i) both of En and Ci have high concentrations in the inner ring for white pigment; (ii) only Ci has a high concentration in the middle ring for black pigment; and (iii) only En has a high concentration in the outer ring for yellow pigment.

Fig. 3 shows the time series of the simulation results of model (13) for wild type at time

$$\{6\ min,\ 30\ min,\ 1\ hr,\ 2\ hr,\ 4\ hr,\ 6\ hr,\ 8\ hr,\ 16\ hr\}.$$

First, the initial peak of En in the inner ring induces the peak of Hh in the inner ring during the early period (around 1 hour). The induced Hh immediately causes an increase in the concentration of Ci in the middle ring and inhibits the concentration of Ci in the inner ring, resulting in a single peak of Ci in the middle ring (around 1 hour). The Ci generated in the middle ring then produces the peak of TGF-β in the middle ring (at about 4 hours). The diffusion of TGF-β immediately increases the production of Ci in the inner ring to generate the peaks of Ci and Wg in the inner ring (around 4 hours). Finally,

both TGF-β and Wg diffuse to the outer wing to generate the peak of En there (around 4 hours). All these interaction are maintained such that the amplitudes of these peaks keep increasing. Eventually, En develops two distinct peaks in the inner and outer rings, Hh has a peak in the inner ring, Ci has peaks in the inner and middle rings, TGF-β has a peak in the middle ring, and Wg has a peak in the inner ring. The high concentrations of En and Ci in the inner ring trigger cells to produce white pigment in the inner ring. The high concentrations of Ci in the middle ring and En in the outer ring activate precursor cells to generate black pigment in the middle ring and yellow pigment in the outer ring, respectively. Additionally, experimental observations show that (i) the concentration of En is high in the inner and outer rings [9], (ii) the concentration of Hh is high in the inner ring [23], (iii) the concentration of Ci is high in the inner and middle ring [23], (iv) the concentration of TGF-β is high in the middle ring [41], and (v) the concentration of Wg is high in the inner ring [41], at the end of eyespot formation process, i.e., 16 hours. Therefore, our mathematical model (13) generates the concentration profiles of these five genes in wild type, which is in accordance with the experimental observation at 16 hours. However, experimental data of the temporal dynamics of these five gene expression concentrations over time are unavailable so far. Thus, we are unable to compare our temporal dynamics simulation (Fig. 3A-G) with experimental observation.

Numerical predictions for null mutants

In this subsection, we use the model (13) to numerically investigate the eyespot pattern when the components En, Hh, Ci, TGF-β, and Wg are knockout separately, i.e., the null mutants, to motivate future experiments for validation.

First, we consider the En null mutants (namely, knockout the En in the model (13)) that we set $E(r,t) \equiv 0$, for $0 \leq r \leq 1$ and for all $t \geq 0$. The simulation result of the En null mutants is shown in Fig. 4. In Fig. 4, when the En is knockout, the concentration of Hh is null everywhere, leading to the result that there is no Ci in the middle ring to generate the black pigment and only a low concentration of TGF-β appears in the middle ring (Notice that the maximal value of TGF-β is around 2×10^{-9} kD/cm which is neglectable, comparing to the wild type in Fig. 3H. The lack of TGF-β eliminates the peak of En in the outer ring, even though the profile of Wg is similar to the wild type. The peaks of En in the inner and outer rings disappear, but Ci still has a peak in the inner ring. Thus, the En null mutants only generate a single inner ring with black pigment, since Ci generates black pigment under the absence of En. This kind of degenerated eyespot is observed from the butterfly, *Vanessa atalanta*. The *Vanessa atalanta* has hindwing eyespots where only the inner ring with black pigment is present as shown in Fig. 9A. Hence, we hypothesize that En deficiency shifts the black pigment to the inner ring and then causes the degenerate eyespot pattern with a single black spot.

Fig. 5 shows the simulation result of Hh null mutants by setting $H(r,t) \equiv 0$, for $0 \leq r \leq 1$ and $t \geq 0$. The En is normally expressed by Dll in the inner ring, but lack of Hh blocks the interaction between En and Ci. Thus, the profiles of Ci, TGF-β, and Wg are the same as the ones shown in En null mutants, i.e., Fig. 4, that the peak of Ci in the middle ring and the peak of En in the outer ring vanish. Hence, the Hh null mutants only have one peak of En and one peak of Ci in the inner ring, resulting in a single white spot.

For the Ci null mutants, we set $C(r,t) \equiv 0$, for $0 \leq r \leq 1$ and $t \geq 0$. The simulation result is displayed in Fig. 6. Since the En works normally, the peaks of En and Hh in the inner ring exist. However, the Ci is vanished everywhere, so there is no peaks of Ci and none of TGF-β and Wg are generated resulting in the loss of En peak in the outer ring. Hence, the Ci null mutants only generate one peak of En in the inner ring resulting in a single white spot.

Based on the results in Figs. 5 and 6, lack of Hh and lack of Ci generate the same degenerated eyespot pattern: a single white spot, which is observed from the species: *Vanessa atalanta* (see Fig. 9A) and *Vanessa altissima* (see Fig. 9B). Thus, we hypothesize that the degenerated single white spot pattern in these two species is caused by the deficiency of Hh or Ci.

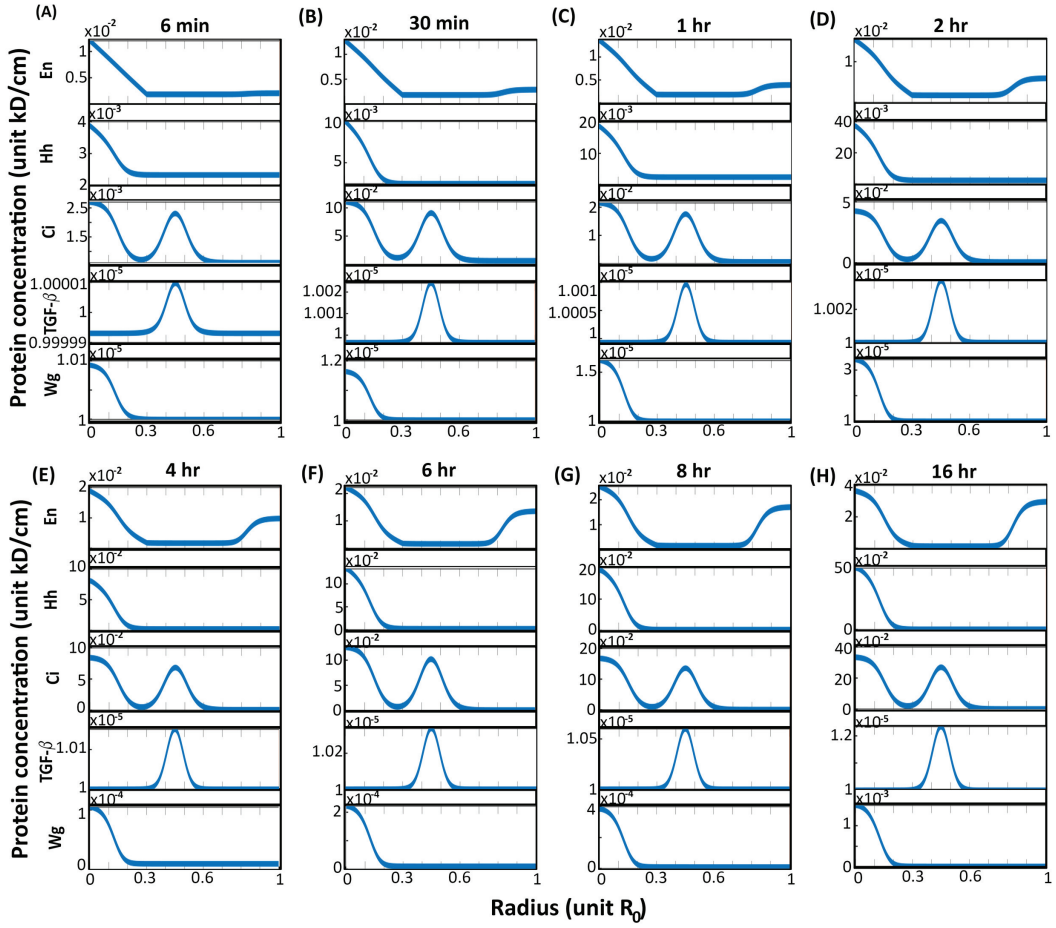

Figure 3. Time series of simulation results for wild type eyespot pattern. (A)-(H) show the simulation results of the model (13) at $\{6\ min,\ 30\ min,\ 1\ hr,\ 2\ hr,\ 4\ hr,\ 6\ hr,\ 8\ hr,\ 16\ hr\}$, respectively. In each figure, the first, second, third, fourth, and fifth rows display the concentrations of En, Hh, Ci, TGF-β, and Wg, respectively. The horizontal and vertical axes represent the radius with unit $R_0(= 0.094\ cm)$ and the concentration of protein with unit kD/cm. For the radius, regions $[0,\ 0.3]$, $[0.3,\ 0.6]$, and $[0.6,\ 1]$ represent the inner ring Ω_{in}, middle ring Ω_{mid}, and outer ring Ω_{out}, respectively. (H) shows the final stage of the eyespot formation, i.e., at 16 hours, that (i) the maximal values of En in Ω_{in} and Ω_{out} are at $3.64603 \times 10^{-2}\ kD/cm$ and $2.96234 \times 10^{-2}\ kD/cm$; (ii) the maximal values of Ci in Ω_{in} and Ω_{mid} are at $3.33815 \times 10^{-1}\ kD/cm$ and $2.69242 \times 10^{-1}\ kD/cm$; and (iii) the maximal values of Hh in Ω_{in}, TGF-β in Ω_{mid}, and Wg in Ω_{in} are at $5.04047 \times 10^{-1}\ kD/cm$, $1.23412 \times 10^{-5}\ kD/cm$, and $1.49298 \times 10^{-3}\ kD/cm$, respectively.

Next, in Fig. 7, we consider the TGF-β null mutants with $T(r,t) \equiv 0$, for $0 \le r \le 1$ and $t \ge 0$. The profiles of En, Hh, and Ci in the inner and middle rings are similar to the wild type. However, knockout of TGF-β blocks the production of Wg such that no interaction between TGF-β and Wg in the outer ring resulting in the loss of En peak in the outer ring. Therefore, the TGF-β null mutants have peaks of En and Ci in the inner ring to produce white pigments in the inner ring and one peak of Ci in the middle ring to generate black pigments in the middle ring. However, cells lose the ability to generate the yellow

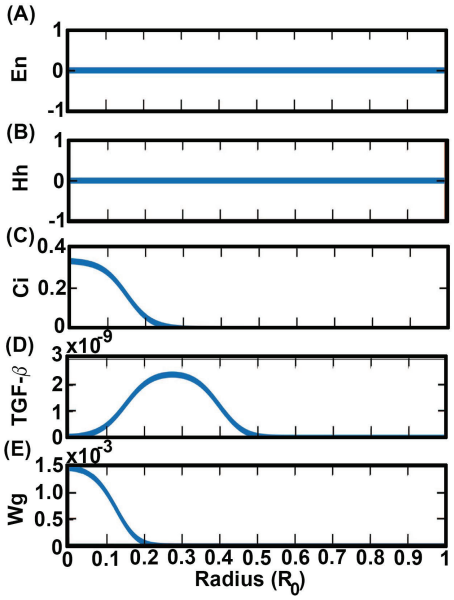

Figure 4. Simulation of En null mutants. (A)-(E) show the concentrations of En, Hh, Ci, TGF-β, and Wg, respectively, at 16 hours, in En null mutants. The horizontal and vertical axes represent the radius with unit $R_0(= 0.094\ cm)$ and concentration of protein with unit kD/cm. The maximal value of TGF-β is at $2.41413 \times 10^{-9}\ kD/cm$.

pigments in the outer ring due to the loss of En peak in the outer ring.

Finally, we consider the Wg null mutants with $W(r,t) \equiv 0$, for $0 \le r \le 1$ and $t \ge 0$ in Fig. 8. The profiles of En, Hh, Ci, and TGF-β in the inner and middle rings are similar to the wild type. However, knockout of Wg loses the interaction between TGF-β and Wg in the outer ring, such that the En peak in the outer ring disappears resulting in loss of the yellow pigments. Hence, the Wg null mutants have the same eyespot pattern as the TGF-β null mutants that the outer yellow ring disappears. This type of degenerated eyespot pattern, losing the outer yellow ring, can be observed from the butterfly, *Chlosyne nycteis* (see Fig. 9C). Combining the results from Figs. 7 and 8, we conjecture that the degenerated pattern with losing the outer yellow ring is caused by loss of TGF-β or Wg signaling.

From the above simulations, we predict the following three types of degenerated patterns in knockout mutants and the results are summarized in Table 3:
(i) deficiency of En causes a single black spot, which can be observed from *Vanessa atalanta*;
(ii) deficiency of Hh or Ci generates a single white spot, which can be observed from *Vanessa atalanta* and *Vanessa altissima*;
(iii) deficiency of TGF-β or Wg loses the outer yellow ring, which can be observed from *Chlosyne nycteis*.

Additionally, the temporal dynamics of these five knockout null mutations are similar to the wild type case shown in Fig. 3 that the time series of Figs. 4-8 show similar profiles of these five components during the whole process. This means that the stable patterns appear at the beginning and maintain during the whole process, so there is no bifurcation or different profiles appear in these five mutations.

Currently, there are a lack of knockout experiments to validate our numerical knockout predictions, so future experiments are required for validation. There are two possible approaches for future experiments. The first approach is to study the phenotype of these null mutants by using the genotype, which includes two types of knockout experiments. One is to knockout or severely knock down one of the components

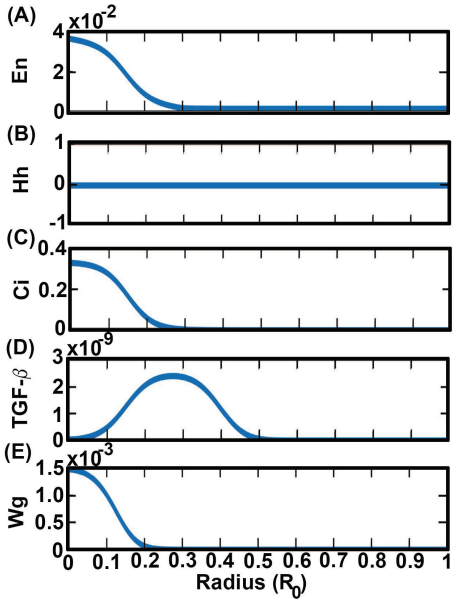

Figure 5. Simulation of Hh null mutants. (A)-(E) show the concentrations of En, Hh, Ci, TGF-β, and Wg, respectively, at 16 hours, in Hh null mutants. The horizontal and vertical axes represent the radius with unit $R_0(= 0.094\ cm)$ and concentration of protein with unit kD/cm. The maximal value of TGF-β is at $2.41413 \times 10^{-9}\ kD/cm$.

$\{En, Hh, Ci, TGF-\beta, Wg\}$ in the embryo [30], through the use of CRISPR, morpholinos, RNAi, or dominant negative viral vector constructs. However, these genetic components play essential roles in the early stages of butterfly development [30], so removing any of these components will lead to embryonic or larval lethality. Thus, it is difficulty to collect gene expression data in late larval and pupal butterfly wings discs form this type of knockout experiment. However, this problem could be solved if the gene knockout process can be performed later in development, perhaps in the late fourth instar or early fifth instar larva stage immediately prior to eyespot determination. The other type of knockout experiment is to knockout essential enzymes for pigment synthesis [30, 71] such that it will not affect essential tissue and organ formation but cells lose the ability to generate the pigments in the corresponding rings. However, this kind of mutant is different from our simulation setting because none of the components of eyespot ring specification are eliminated, and hence it cannot be used to validate our prediction results. An alternative to study of knockout or knock down experiments is to study the genotype by using the phenotype from the selected lines. For the existing experiments in *Bicyclus anynana*, there are two selected lines: one is no black ring (c.f. [9]) and the other is no yellow ring (c.f. [3] and *Chlosyne nycteis* in Fig. 9D). The difference of gene expression between the selected lines and wild type can be used to study the key factors for generating the deficient eyespot pattern.

Sensitivity analysis

(We change everything in this Section.)

In this section, we perform the sensitivity analysis created by S. Marino et al. in [36] to investigate the robustness of the model outcomes and prevent the over fitting issue, by analyzing how the parameter values affect the wild type (*Bicyclus anynana*) eyespot pattern (namely, the peaks of En and Ci in different rings) and the variations of all components. We will first apply the sensitivity analysis on three

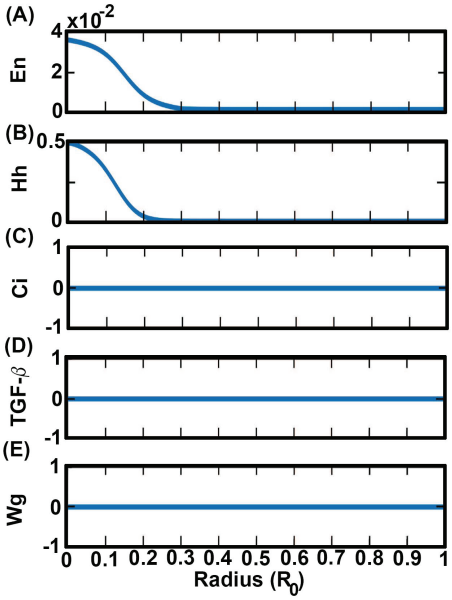

Figure 6. Simulation of Ci null mutants. (A)-(E) show the concentrations of En, Hh, Ci, TGF-β, and Wg, respectively, at 16 hours, in Ci null mutants. The horizontal and vertical axes represent the radius with unit $R_0(= 0.094\ cm)$ and concentration of protein with unit kD/cm.

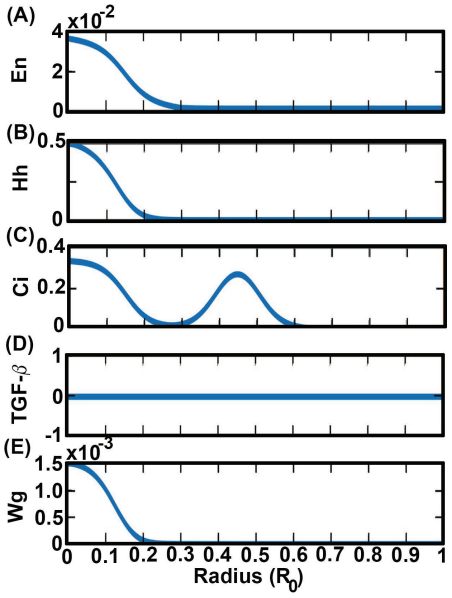

Figure 7. Simulation of TGF-β null mutants. (A)-(E) show the concentrations of En, Hh, Ci, TGF-β, and Wg, respectively, at 16 hours, in TGF-β null mutants. The horizontal and vertical axes represent the radius with unit $R_0(= 0.094\ cm)$ and concentration of protein with unit kD/cm.

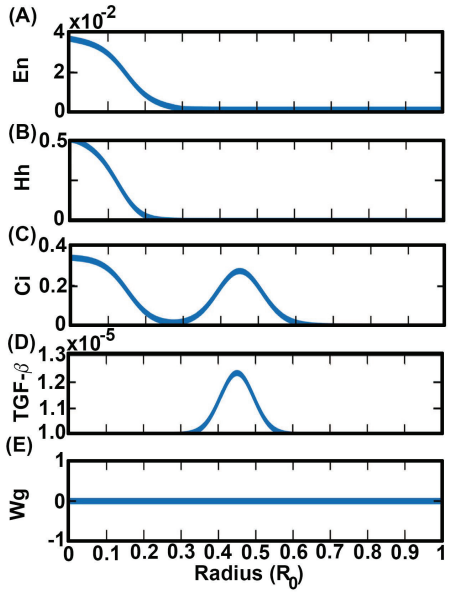

Figure 8. Simulation of Wg null mutants. (A)-(E) show the concentrations of En, Hh, Ci, TGF-β, and Wg, respectively, at 16 hours, in Wg null mutants. The horizontal and vertical axes represent the radius with unit $R_0(= 0.094\ cm)$ and concentration of protein with unit kD/cm.

Table 3. Eyespot patterns for different null mutants. In the species row, A-D represent the wild type of *Bicyclus anynana*, *Vanessa atalanta*, *Vanessa altissima*, and *Chlosyne nycteis*, respectively. The named pattern row shows the cartoon of the expected eyespot pattern. The actual eyespot patterns are shown in Fig. 9.

Mutant type	wild type	null En	null Hh	null Ci	null TGF-β	null Wg
En peak in Ω_{in}	presence	absence	presence	presence	presence	presence
pigment in Ω_{in}	white	black	white	white	white	white
Ci peak in Ω_{mid}	presence	absence	absence	absence	presence	presence
pigment in Ω_{mid}	black	null	null	null	black	black
En peak in Ω_{out}	presence	absence	absence	absence	absence	absence
pigment in Ω_{out}	yellow	null	null	null	null	null
pattern						
species	A	B	B, C	B, C	D	D

cases to study the wild type pattern: (i) the peak of En in the outer ring, (ii) the peak of Ci in the inner ring, and (iii) the peak of Ci in the middle ring. Next, for the model robustness, we perform the sensitivity analysis on all components in all rings to broadly investigate how the parameter values affect the gene expression pattern.

The concept of sensitivity analysis mentioned in [36] is to evaluate how the uncertainty and variations in model outputs are correlated to parameter values, by using the Latin hypercube sampling (LHS) and partial rank correlation coefficient (PRCC). For each parameter, the LHS is a sampling method

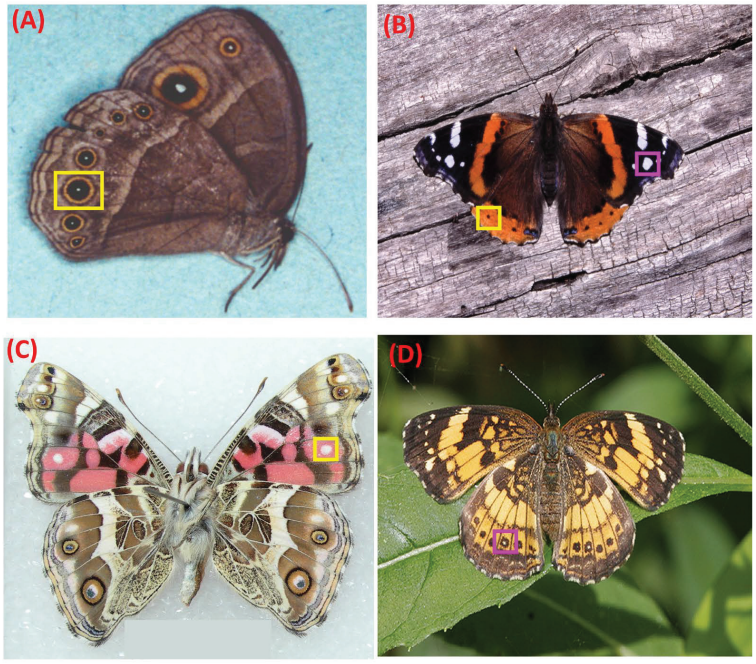

Figure 9. Images of butterfly. (A)-(D) show the images of butterflies: wild type of *Bicyclus anynana*, *Vanessa atalanta*, *Vanessa altissima*, and *Chlosyne nycteis*, respectively. In (A), the yellow box indicates the eyespot of wild type. In (B), the yellow and pink boxes show the black inner ring and white inner rings, respectively, in *Vanessa atalanta*. The yellow box in (C) display the white inner ring in *Vanessa altissima*, and the pink box in (D) indicates the white inner ring and black middle ring in *Chlosyne nycteis*.

that generates uniform parameter value distributions divided into N equal probability intervals, where N is the sample size. Each interested parameter will be sampled independently by using LHS. All the samples are collected to generate a set $\{P_1, P_2, \cdots, P_N\}$ and each P_i includes the values for all interested parameters. Next, substitute each set P_i into the parameter values of the model to generate the model outcomes $\{y_1, y_2, \cdots, y_N\}$. The value of PRCC between the parameter values $\{P_1, P_2, \cdots, P_N\}$ and model outcomes $\{y_1, y_2, \cdots, y_N\}$ shows the robust sensitivity for their nonlinear and monotonic relationships. Thus, a parameter with positive PRCC to the model outcome and p-value smaller than 0.05 represents that the model outcome increases as the value of the parameter increases, whereas a parameter with negative PRCC to the model outcomes and p-value smaller than 0.05 accounts for an opposite result that the model outcome decreases as the value of the parameter increases. However, for a parameter with small $|PRCC|$ and p-value larger than 0.05, then the parameter value does not have significant effect on the model outcome. Thus, the sensitivity analysis can also be used to study the over fitting issue. If most parameters are with small $|PRCC|$ and p-value larger than 0.05, then the model outcome is not sensitive to most parameter values which means that the dynamics of the model is robustness.

To analyze how the parameter values affect the peak appearance in each ring, we define the following

functions

$$\begin{aligned}\hat{X}_{in}(t) &:= \max\{X(r,t) : 0 \le r \le 0.3\},\\ \hat{X}_{mid}(t) &:= \max\{X(r,t) : 0.3 \le r \le 0.6\},\\ \hat{X}_{out}(t) &:= \max\{X(r,t) : 0.6 \le r \le 1\},\end{aligned}$$

and

$$X_{in}(t) = \frac{\hat{X}_{in}(t)}{X(0.3,t)},\ X_{mid}(t) = \frac{\hat{X}_{mid}(t)}{X(0.3,t)+X(0.6,t)},\ X_{out}(t) = \frac{\hat{X}_{out}(t)}{X(0.6,t)}, \tag{14}$$

with $X \in \{E,\ H,\ C,\ T,\ W\}$. Since we only focus on the end of the development, we take $t = 16$ hours in this section. By using the functions in Eq. (14), if $X_j(t) > 1$ with $X \in \{E,\ H,\ C,\ T,\ W\}$ and $j \in \{in,\ mid,\ out\}$, then there exists at least one peak of X in the ring j, at time t. For each parameter, we generated 10000 samples individually, via the Latin hypercube sampling, with $dt = 0.01$ minutes and $dr = 0.001 \times R_0$. We choose these parameters in the range from 0.5 to 2 fold of their baseline values. The Table 4 shows the baselines, ranges, and units of the parameters for each parameter.

Our simulations show that the following functions are always smaller than one under all parameter samples,

$$E_{mid}(t),\ H_{mid}(t),\ H_{out}(t),\ C_{out}(t),\ T_{in}(t),\ T_{mid}(t),\ T_{out}(t),\ W_{mid}(t),\ W_{out}(t).$$

This result indices that there is no peak of Hh, Ci, TGF-β, and Wg in the outer ring and TGF-β in the inner ring, and we cannot make any conclusion of the peak in the middle ring for En, Hh, TGF-β, and Wg. Therefore, in the following, we only focus on the En peaks in the inner and outer rings, Hh peak in the inner ring, Ci peaks in the inner and middle rings, and Wg peak in the inner ring. The PRCCs and the p-values of parameters for these cases are shown in Table 5. For the considered $X_j(t)$, a parameter with a negative (resp. positive) PRCC and p-value smaller than 0.05 indicates that increasing this parameter will decrease (resp. increase) the ratio $X_j(t)$ and hence reduces (resp. increases) the chance to generate the peak of X in the ring j.

In the following, we will use the PRCCs in Table 5 to investigate i) how the parameter values affect the peaks in wild type, ii) how the diffusion and degradation rates of each gene affect the peaks, and iii) how the parameter values affect the remainder peaks.

Wild type pattern.

The eyespot pattern in the wild type requires a peak of En and a peak of Ci in the inner ring for white pigment, a peak of Ci in the middle ring for black pigment, and a peak of En in the outer ring for yellow pigment. According to the initial condition, the peak of En in the inner ring always exists. Thus, we only need to consider three cases: (i) the peak of En in the outer ring, (ii) the peak of Ci in the inner ring, and (iii) the peak of Ci in the middle ring. We choose the parameters λ_E and α_E for case (i), $\lambda_C,\ \alpha_H$, and α_C for case (ii), and $\alpha_C,\ \mu_E,\ \alpha_E,\ \alpha_H,\ \lambda_C$, and d_H for case (iii). We then use the PRCCs with p-value corresponding to the ratios $E_{out}(t)$ in case (i), $C_{in}(t)$ in case (ii), and $C_{mid}(t)$ in case (iii), at $t = 16$ hours.

In case (i), the PRCC of α_E and λ_E are positively correlated to $E_{out}(t)$that increasing α_E or λ_E promotes the generation of En peak in the outer ring. Increasing α_E generates more En as a source of other components and hence increases the amount of Wg to generate more En in the outer ring. Increasing λ_E enhances the effect from the interaction between TGF-β and Wg in the outer ring, such that En is more sensitive to TGF-β and Wg for generating the peak in the outer ring.

In case (ii), the PRCCs of α_H and α_C are negatively correlated and λ_C is positive correlated to $C_{in}(t)$. Increasing α_H promotes the production of Hh in the inner ring resulting in more inhibition on Ci in the inner ring. On the other hand, increasing α_C enhances the production of Ci in the middle ring. However, the negative feedback of Ci then inhibits the production of Hh in the inner ring and hence increases the

Table 4. Parameters chosen for LHS. This table shows the LHS ranges (in the third column) of the selected parameters (in the first column). For each parameter, we use the baseline (i.e., the second column) to create the sampling range by including the values between the 0.5 and 2 fold of the baseline).

Parameter	Baseline	Range	Unit
d_H	2.97017×10^{-7}	$[1.4851, 5.9403] \times 10^{-7}$	cm^2/min
d_T	3×10^{-7}	$[1.5, 6] \times 10^{-7}$	cm^2/min
d_W	2.91519×10^{-7}	$[1.4576, 5.8304] \times 10^{-7}$	cm^2/min
μ_E	3.85082×10^{-4}	$[1.9254, 7.7016] \times 10^{-4}$	$/min$
μ_H	1.38629×10^{-2}	$[0.6931, 2.7726] \times 10^{-2}$	$/min$
μ_C	9.24196×10^{-3}	$[4.6210, 18.4839] \times 10^{-3}$	$/min$
μ_T	5.77623×10^{-3}	$[2.8881, 11.5525] \times 10^{-3}$	$/min$
μ_W	1.15525×10^{-3}	$[0.5776, 2.3105] \times 10^{-3}$	$/min$
N_0	1	$[0.5, 2]$	kD/cm
α_E	$(3.56201 \times 10^{-2})N_0$	$[1.7810, 7.1240] \times 10^{-2}$	kD/cm
α_H	2.18247×10^{-2}	$[1.0912, 4.3649] \times 10^{-2}$	$/min$
α_C	1.20978×10^{-3}	$[0.6049, 2.4196] \times 10^{-3}$	$/min$
α_T	1.89385×10^{-5}	$[0.9469, 3.7877] \times 10^{-5}$	$/min$
α_W	9.46923×10^{-5}	$[4.7346, 18.9385] \times 10^{-5}$	$/min$
λ_E	$\frac{3.56201 \times 10^{-2}}{N_0}$	$[1.7810, 7.1240] \times 10^{-2}$	$cm/kD/min$
λ_C	$352.35N_0$	$[176.1750, 704.7000]$	kD/cm
k_H	$1/(4N_0)$	$[0.125, 0.5]$	cm/kD
k_C	$1/(932N_0)$	$[0.0005, 0.0021]$	cm/kD

production of Ci in the inner ring, resulting in reducing the peak of Ci in the inner ring. A larger value of λ_C increases the concentration of Ci in the inner ring resulting in generating the peak in the inner ring.

In case (iii), the PRCCs of α_C and μ_E are positively correlated and the PRCCs of α_E, α_H, λ_C and d_H are negatively correlated to $C_{mid}(t)$. Increasing α_C promotes the Ci peak generation by Hh in the middle ring. Moreover, increasing μ_E reduces the amount of En and Hh resulting in reduction of Ci in the middle ring including $C(0.6, t)$. Hence, it could increase the amount $C_{mid}(t)$. On the other hand, increasing α_E or α_H enhances the production of Hh and then produces more Ci in the middle ring at the beginning. However, the negative feedback of Ci will reduce the amount of Ci in the middle ring and then reduce the chance to generate the peak in the middle ring. The Hh diffuses faster under larger d_H, so there is less Hh in the middle ring to activate Ci production at the beginning. Similarly, the negative feedback of Ci will increase the amount of Ci in the middle ring eventually. A higher λ_C generates more Ci in the inner ring and hence reduce the ratio between Ci in the middle ring and at the boundary, i.e., $C_{mid}(t)$.

Effect from the diffusion and degradation rates.

For butterflies growing in different season, the temperature affects the eyespot size [8]. Although the eyespot size is fixed in our model, we can still study how the temperature affects the peaks of the five genes in our model. Based on basic principle in physics, a higher temperature accelerates the motion of particles resulting in increasing of the diffusion rate. On the other hand, a higher temperature could make the protein ligand degrades quicker ([25, 42, 72] for Wg and [42] for TGF-β). Thus, we assume that when the temperature increases, the diffusion rates of Hh, TGF-β and Wg increase and the half-life of En. Hh, Ci, TGF-β, and Wg decrease (i.e., the degradation rates increase). We then use the PRCCs of the diffusion and degradation rates to investigate how the temperature affects the peak of these five

Table 5. The PRCC and p-value of parameters form sensitivity analysis. This table shows the PRCC (in the fourth column) between the parameter (in the third column) and model outcome (in the second column), with p-value (in the last column) smaller than 0.05. A parameter with positive PRCC (resp. negative PRCC) and p-value smaller than 0.05 means that the model outcome increases (resp. decreases) as the parameter value increases.

Case	Model outcome	Parameter	PRCC	p-value
En peak in Ω_{in}	$E_{in}(t)$	α_E	0.99657	< 0.05
En peak in Ω_{in}	$E_{in}(t)$	μ_E	0.94149	< 0.05
En peak in Ω_{out}	$E_{out}(t)$	λ_E	0.99660	< 0.05
En peak in Ω_{out}	$E_{out}(t)$	α_E	0.94169	< 0.05
Hh peak in Ω_{in}	$H_{in}(t)$	α_H	0.96567	< 0.05
Hh peak in Ω_{in}	$H_{in}(t)$	α_E	0.94460	< 0.05
Hh peak in Ω_{in}	$H_{in}(t)$	d_H	-0.39519	< 0.05
Hh peak in Ω_{in}	$H_{in}(t)$	μ_E	-0.46706	< 0.05
Ci peak in Ω_{in}	$C_{in}(t)$	λ_C	0.95999	< 0.05
Ci peak in Ω_{in}	$C_{in}(t)$	α_H	-0.33231	< 0.05
Ci peak in Ω_{in}	$C_{in}(t)$	α_C	-0.95766	< 0.05
Ci peak in Ω_{mid}	$C_{mid}(t)$	α_C	0.9453	< 0.05
Ci peak in Ω_{mid}	$C_{mid}(t)$	μ_E	0.19045	< 0.05
Ci peak in Ω_{mid}	$C_{mid}(t)$	α_E	-0.11835	< 0.05
Ci peak in Ω_{mid}	$C_{mid}(t)$	d_H	-0.34804	< 0.05
Ci peak in Ω_{mid}	$C_{mid}(t)$	α_H	-0.83661	< 0.05
Ci peak in Ω_{mid}	$C_{mid}(t)$	λ_C	-0.90735	< 0.05
Wg peak in Ω_{in}	$W_{in}(t)$	λ_C	0.96386	< 0.05
Wg peak in Ω_{in}	$W_{in}(t)$	α_W	0.95397	< 0.05
Wg peak in Ω_{in}	$W_{in}(t)$	d_W	-0.20476	< 0.05

components.

About the diffusion rates, as shown in Table 5, the PRCCs of d_H are negatively correlated to the Hh peak in the inner ring and Ci peak in the middle ring. This result indicates that for a larger diffusion rate d_H, the Hh diffuses faster and the profile of Hh is flatter everywhere resulting in reducing the peak of Hh in the inner ring and reducing the effect on Ci in the middle ring. On the other hand, the PRCC of d_W is negatively correlated to the Wg peak in the inner ring. Similar explanation can be applied to the effect of d_W on the peak of Wg in the inner ring. Therefore, when the temperature is higher, these diffusion rates d_H and d_W increase resulting in reducing the peaks of Hh and Wg in the inner ring and the peak of Ci in the middle rings.

About the degradation rates, we found that the degradation rate of En μ_E is positively correlated to the En peaks in the inner ring and Ci peak in the middle ring, whereas μ_E is negatively correlated to Hh peaks in the inner and middle rings. For a high μ_E, it reduces the amount of En in the region $0 < r \leq 1$ and hence reduces the amount of Hh in the same region, resulting in larger $E_{in}(t)$ (due to lower $E(0.3, t)$) and lower H_{in} (due to lower $H(r, t)$ for $0 \leq r \leq 0.3$). Moreover, the reduction of Hh also inhibits the amount of Ci in the middle ring at the beginning. However, the negative feedback of Ci eventually increases Ci in the middle ring. On the other hand, the degradation rate of TGF-β μ_T is negatively correlated to the En peak in the outer ring. Increasing μ_T decreases the amount of TGF-β to activate with Wg to generate En in the outer ring. Additionally, the degradation rate of Hh μ_H is positively correlated to the Hh peak in the inner ring. A higher value of μ_H reduces the amount of Hh in the region $0 < r \leq 1$ at the beginning. However, the negative feedback will increase the value of Hh in

the inner ring eventually.

Other cases.
In this part, we will focus on the cases and parameters that are not discussed previously. About the peaks of Hh, α_E and α_H are positively correlated to the peak in the inner ring, since a higher amount of α_E or α_H promotes the production of Hh in the inner ring. About the peaks of Wg, the PRCCs of α_W and λ_C are positively correlated to the peak of Wg in the inner ring. Increasing α_W enhances the amount of Wg in the inner ring. Increasing λ_C enhances the amount of Ci in the inner ring, resulting in promotion of the peak of Wg in the inner ring.

Overall, our sensitivity analysis shows that the model (13) can generate peaks of En in the inner and outer rings, Hh in the inner ring, Ci in the inner and middle rings, and Wg in the inner ring, if no gene is removed. However, the model (13) cannot generate peaks of Hh, Ci, TGF-β, and Wg in the outer ring and the peak of TGF-β in the inner ring, when the parameter values are within half and two fold of their baselines. Although, we cannot make conclusion about the peak of TGF-β in the middle ring from the sensitivity analysis, the model structure guarantees the appearance of TGF-β peak in the middle ring due to the second term in Eq. (8). Additionally, our results cannot make conclusion about the peaks of En, Hh, and Wg in the middle ring. If we exclude the appearance of these three peaks, then our model is robust to generate the wild type pattern, namely, Fig. 3H. However, if we assume these three peaks can appear, then we have six situations shown in Fig. 10. Recall that cells in the inner ring generate white pigment under the high concentrations of En and Ci, cells in the middle ring show the black pigment under the high concentration of Ci and white under the high concentrations of En and Ci, and cells in the outer ring produce the yellow pigment under the high concentration of En. Thus, Fig. 10 provides two patterns: (i) white inner ring, black middle ring, and yellow outer ring (protein concentrations are shown in Figs. 10A, 10B, and 10C and the corresponding eyespot cartoon is shown in Fig. 10D) and (ii) white inner and middle rings and yellow outer ring (protein concentrations are shown in Figs. 10E, 10F, and 10G and the corresponding eyespot cartoon is shown in Fig. 10H). The pattern in case (i) equals to the wild type and the pattern in case (ii) can be found from a mutant line of *Bicyclus anynana* butterflies (Goldeye) (see the Fig. 3F in [9]).

Discussion

In this work, we constructed a mathematical model including the proteins En, Hh, Ci, TGF-β, and Wg to generate their dynamics in the inner, middle, and outer rings of eyespots. Our model captured the dynamics of these five components observed in the wild type *Bicyclus anynana* and *Junonia coenia* butterflies [9,41] that the concentration of En had peaks in the inner and outer rings, and the concentration of Ci had peaks in the inner and middle rings. The presences of En peak and Ci peak in the inner ring triggered the cells in the inner ring to display the white pigments. The single Ci peak in the middle ring and single En peak in the outer ring induced the black pigments in the middle ring and yellow pigments in the outer ring, respectively. Thus, our numerical simulations were in accordance with existing experimental observations in *Bicyclus anynana* and *Junonia coenia* [9,41].

We also investigated the eyespot patterns of the null mutants. Our simulation predicted three degenerated eyespot patterns. (i) The type I pattern displayed a single black spot which was caused by En protein deficiency. (ii) The type II pattern showed a single white spot which was generated by the loss of Hh or Ci proteins. (iii) The type III pattern lost the outer yellow ring which was caused by deficiency of TGF-β or Wg proteins. These predictions suggested the mechanism for generating the degenerated eyespot patterns observed from the species *Vanessa atalanta* (single black spot or single white spot), *Vanessa altissima* (single white spot), and *Chlosyme nycteis* (loss of the outer yellow ring). The simulation predictions for the null mutants were purely predictive, and were required further experiments for validation. First, we could manipulate the genotype by implementing CRISPR, morpholinos, RNAi, or

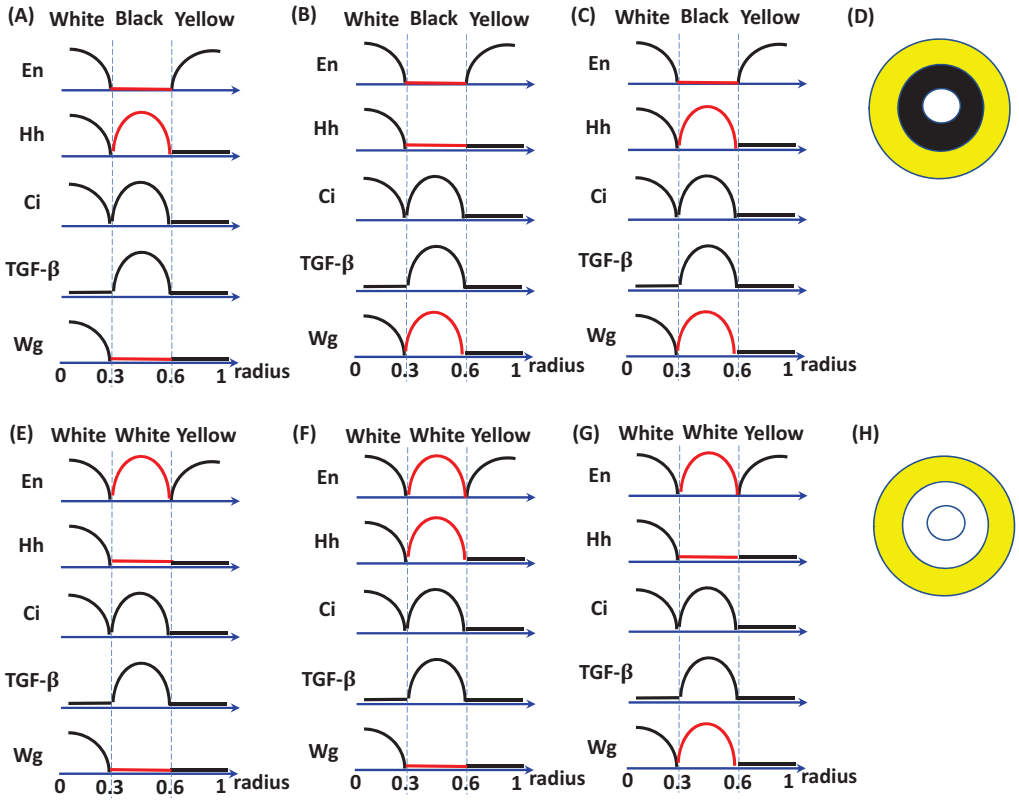

Figure 10. All combinations of the peaks in middle ring. (A)-(C) and (E)-(G) show different combinations of peaks of En, Hh, and Wg in the middle rings. The black curve represents the peaks appear in all cases, while the red curve displays the peaks appear under certain condition. The expected pigments are listed at the top of each figure. The cartoons in (D) and (H) show the expected eyespot patterns for the protein concentrations in (A)-(C) and (E)-(G), respectively.

virus vectors containing dominant negative constructs to knockout or knock down of the target gene or enzyme to study the resulting phenotype. In this case, we could either knockout one of the components $\{En, Hh, Ci, TGF-\beta, Wg\}$ after the formation of major organs and before the larva stage, or knockout the enzyme for pigment synthesis to remove the pigment in each wing directly. Second, we could utilize the phenotype from the selected lines with eyespot pattern deficiency to study the genotype. In *Bicyclus anynana*, two selected lines, no black ring or no yellow ring, could be used to investigate the key factors for the deletions of black and yellow pigment synthesis. However, among these potential knockout experiments, only the one that knockout one gene among $\{En, Hh, Ci, TGF-\beta, Wg\}$ right before the larva stage was in accordance with our simulation setting and could be used to validate our predictions.

Additionally, our parameter values were based on the assumption of the similarity of molecular information among insects with wings, *Drosophila*, and butterflies. Thus, we further performed the sensitivity analysis to study how these parameter values correlated to the eyespot pattern. Our results of sensitivity analysis suggested that increasing the value of λ_E or α_E promoted the yellow pigment formation in the outer ring. Moreover, increasing the value of α_E, μ_E, or λ_C or reducing the value of α_H or α_C promoted the white pigment formation in the inner ring. On the other hand, enhancing α_C or μ_E or reducing α_E, α_H, λ_C, and d_H promoted the black pigment formation in the middle ring. We also investigated

how the changes of diffusion and degradation rates caused by temperature affected the peak formation. Furthermore, the model robustness was demonstrated by the sensitivity analysis. These findings helped us understand the detailed reactions among these five proteins at different locations inside the eyespot. Based on our simulation predictions of null mutants, further experiments can be performed on specific species to verify our hypotheses.

In Fig. 3, we found that the peaks of En and Ci appear in the following order: peak of En in the inner ring, followed by the peaks of Ci in the middle and inner rings, and then the peak of En in the outer ring. Thus, we hypothesized that the cells making white pigment in the inner ring and making black pigment in the middle ring were activated at the same time, and then the precursor cells of yellow pigment in the outer ring were activated later. However, experimental observation showed that the white inner ring and yellow outer ring appear first and then the black middle ring appears later [33]. The difference between the appearance order of gene expression peaks and visible pigment formation can be easily explained by considering the various functions of the black melanin pigment. Besides producing black color patterns, black melanin pigment also has an important role in wing cuticle sclerotization (hardening), which is essential for producing a flat stiff wing surface capable of supporting flight. For this reason, the substrates required to produce black melanin pigment are made available to the wing late in development, long after the cells which produce black pigment in the eyespot are specified (after the process described in Fig. 2), and hence this would delay the formation of black pigment.

In this work, we only used chemical reactions among the gene expression products to describe the eyespot formation. However, recently there were many findings showing that not only chemical reactions, but also cellular and mechanical processes could actively drive pattern formation during the development. From mathematical perspective, the authors in [19, 22, 37] provided different mathematical approaches to incorporate the effect from cellular and mechanical processes. For instance, the Turings reaction-diffusion model and molecular and cellular mechanical processes mentioned in [22] are similar mathematical methods that were used to generate bifurcation for spots, stripes, and oscillation patterns. The methods mentioned in [37] provided an extension of Turings reaction-diffusion model. The idea mentioned in [19] discussed how system motifs, such as how the negative feedback loop generates oscillation pattern, affect the model dynamics. Therefore, these were general approaches that work for most reactions and were not restricted to chemical reaction, cellular or mechanical processes in development. From biological perspective, cellular and mechanical processes also influence eyespot formation. For instance, as an example of a cellular process, in the eyespot region, cells located in the inner, middle, and outer rings are not able to move to different rings during the eyespot formation process likely due to differences in cell adhesion [38], and the development in each ring express different biosynthetic pathways to form different pigments [33]. Mathematical models need to include the information about individual cell behavior or cell movement to capture this kind of cellular process. On the other hand, ectopic eyespots can also be induced as part of the wound healing process following mechanical disruption of developing wing tissue (i.e., a mechanical process) [7]. Mechanistically, after developing wing tissue is damaged, one by-product of the wound healing process is the upregulation of gene products such as Dll, which promotes cell division. At the same time, as seen in Fig. 2, Dll is also directly upstream of the network responsible for eyespot ring formation, initiating the production of an ectopic eyespot [40]. Our model is related to the effects of this mechanical process, since our model captured the downstream behavior of Dll and the genes that respond to Dll. Thus, if we extend the model to include the gene expression products in the wound healing process, then the model can be also used to study how at least some mechanical processes affect eyespot formation.

Acknowledgements

Liao and Marcus are supported by the Discovery Grant of the Natural Sciences and Engineering Research Council of Canada [grant number RGPIN-2020-07097 for Kang-Ling Liao] [grant number RGPIN-2016-

06012 for Jeffery Marcus]. Chang and Wang are supported in part by the Ministry of Science and Technology of Taiwan [grant number MOST 109-2115-M-002-001-MY3 for Jenn-Nan Wang].

Methods: Parameter estimation

In the following, to avoid over fitting, we estimate the parameter values by using experimental data from *Bicyclus anynana*, *Drosophila*, cockroach and mice shown in Tables 6, 7, and 8. Therefore, all the parameter values are based on experimental data. Although some parameter values are based on the data from different species (such as cockroach and mice), our sensitivity analysis provides a method to predict the simulation result when the data from butterflies become available.

Estimates of the diffusion coefficients.

The diffusion rate of component X is defined as

$$d_X = 8.34 \times 10^{-8} (\frac{\tilde{T}}{\mu M_X^{1/3}}) \ cm^2 \ s^{-1}, \tag{15}$$

where $\tilde{T}$ and μ are the temperature and solution viscosity [12]. We take

$$d_T = 0.5 \ \mu m^2/s = 5 \times 10^{-9} \ cm^2/s = 3 \times 10^{-7} \ cm^2/min \tag{16}$$

which is the diffusion rate of dpp in [12]. From the molecular weights of Wg, Hh, and TGF-β shown in Table 6, we have the following molecular weight ratio among these three proteins

$$M_W : M_H : M_T = 44.76 : 42.32 : 41.07,$$

where M_W, M_H, and M_T are the molecular weights of Wg, Hh, and TGF-β, respectively. Combining this ratio with the equation Eq. (15), we have

$$d_W = (\frac{M_T}{M_W})^{1/3} d_T = (\frac{41.07}{44.76})^{1/3} \times 3 \times 10^{-7} \ cm^2/min = 2.91519 \times 10^{-7} \ cm^2/min, \tag{17}$$

$$d_H = (\frac{M_T}{M_H})^{1/3} d_T = (\frac{41.07}{42.32})^{1/3} \times 3 \times 10^{-7} \ cm^2/min = 2.97017 \times 10^{-7} \ cm^2/min. \tag{18}$$

Estimates of the degradation rates.

We use the linear equation

$$\frac{d}{dt} x(t) = -kx(t) \tag{19}$$

and the half-life listed in Table 7 to obtain the following degradation rates

$$\begin{aligned}
\text{degradation rate of En}=\mu_E &= \ln 2/(1800 \ min) = 3.85082 \times 10^{-4} \ /min, \\
\text{degradation rate of Hh}=\mu_H &= \ln 2/(50 \ min) = 1.38629 \times 10^{-2} \ /min, \\
\text{degradation rate of Ci}=\mu_C &= \ln 2/(75 \ min) = 9.24196 \times 10^{-3} \ /min, \\
\text{degradation rate of TGF-}\beta=\mu_T &= \ln 2/(600 \ min) = 1.15525 \times 10^{-3} \ /min, \\
\text{degradation rate of Wg}=\mu_W &= \ln 2/(120 \ min) = 5.77623 \times 10^{-3} \ /min.
\end{aligned}$$

Notice that we use the half-life data of En, Hh, and Wg from cockroach and mice (shown in Table 7) to estimate the degradation rates μ_E μ_H, μ_W, which may not be able to capture the real situation in butterflies. Thus, we included these three degradation rates into the sensitivity analysis to study how

their values affect the result. Our sensitivity analysis result shows that only μ_E has positive correlation to the En peak in the inner ring and Ci peak in the middle ring and has negative correlation to the Hh peak in the inner ring (Table 5). Therefore, when the half-life data of En in insects with wings becomes available, our result still be able to predict the behavior. For example, if the half-life of En in butterflies is shorter than the one in mice (namely, the degradation rate of En in butterflies is bigger then the one in mice), then the probability of having En peak in the inner ring and Ci peak in the middle ring is higher, but the probability of having Ci peak in the middle ring is lower. Moreover, the other two degradation rates μ_H and μ_W do not have significant effect on any peaks in any rings. Thus, if the half-life of Hh and Wg in butterflies is different to cockroach and mice, it will not change the simulation outcome of our model, since the values of μ_H and μ_W will not affect the model outcome.

Estimate the steady states for all components.
To estimate the steady states of all proteins, En, Hh, Ci, TGF-β (or dpp), and Wg, we assume that the mRNA is a proportion of its protein. Thus, we use the transcript amount of mRNA listed in Table 8 to estimate the ratio of En, Hh, Ci, TGF-β (or dpp), and Wg mRNA. Next, we use the mRNA amounts of these five components to estimate the ratio among these five proteins.

Since dpp and Wg are not detected in eyespots (see Table 8), we assume that the proportions of dpp and Wg are relative small (say 1), and then we have the following ratio

$$En : Hh : Ci : dpp : Wg = 185 : 233 : 61 : 1 : 1.$$

We then assume that the steady states of all components are

$$En = 185N_0,\ Hh = 233N_0,\ Ci = 61N_0,\ dpp = N_0.\ Wg = N_0, \tag{20}$$

for some estimated N_0. For simplicity, we take $N_0 = 1\ kD/cm$ (The model generates similar results for wild type and null mutants if $10^{-3} \leq N_0 \leq 2$. Results are now shown here).

To estimate the parameter values of the model (13), we consider the following simplified model constructed by Ordinary Differential Equations (ODEs).

$$\frac{dE}{dt} = \alpha_E + \lambda_E T \cdot W - \mu_E E \tag{21}$$

$$\frac{dH}{dt} = \frac{\alpha_H E}{1 + k_H T} - \mu_H H \tag{22}$$

$$\frac{dC}{dt} = \frac{\lambda_C}{1 + k_C H} + \alpha_C H - \mu_C C \tag{23}$$

$$\frac{dT}{dt} = \alpha_T C - \mu_T T \tag{24}$$

$$\frac{dW}{dt} = \alpha_W C - \mu_W W. \tag{25}$$

In the following, we use the half-life listed in Table 7 and the steady state in Eq. (20) to estimate the parameters of model (13).

Estimate the parameters of Eq. (21).
For simplicity, in the Eq. (21), we assume that the amounts of α_E and $\lambda_E \cdot T \cdot W$ are similar, so

$$\begin{aligned}\lambda_E &= \frac{1}{2}\frac{\mu_E \cdot E}{T \cdot W} = \frac{(3.85082 \times 10^{-4}/min) \times 185N_0}{2N_0^2} = \frac{3.56201 \times 10^{-2}/min}{N_0} = 3.56201 \times 10^{-2}\ cm/kD/min,\\ \alpha_E &= \frac{1}{2}\mu_E \cdot E = \frac{1}{2} \times (3.85082 \times 10^{-4}/min) \times 185N_0 = (3.56201 \times 10^{-2}/min)N_0\\ &= 3.56201 \times 10^{-2}\ kD/cm/min.\end{aligned}$$

Estimate the parameters of Eq. (22).
For the steady state of the Eq. (22), we assume that the inhibition from T is around 4/5, i.e., $\frac{1}{1+k_H T} = 4/5$, and hence

$$\alpha_H = \frac{5}{4}(\mu_H \cdot H)/E = 1.25 \times (1.38629 \times 10^{-2}/min) \times (233N_0/185N_0) = 2.18247 \times 10^{-2}/min$$

and

$$\frac{1}{1+k_H T} = \frac{4}{5} \ \Rightarrow\ k_H = 1/(4N_0) = 0.25\ cm/kD.$$

Estimate the parameters of Eq. (23).
For the steady state of the Eq. (23), we assume that $\alpha_C \frac{1}{1+k_C H}$ and $\alpha_C \cdot C$ have similar amount and the inhibition from H is 4/5. Thus, we have

$$\begin{aligned}\alpha_C &= \frac{1}{2}(\mu_C \cdot C)/H = \frac{1}{2}(9.24196 \times 10^{-3}/min) \times (61N_0/233N_0) = 1.20978 \times 10^{-3}/\min,\\ \lambda_C &= \frac{5}{4}(\frac{1}{2}\mu_C \cdot C) = \frac{5}{8}(9.24196 \times 10^{-3}/min) \times 61N_0 = 352.35N_0/min = 352.35\ cm/kD/min,\end{aligned}$$

and

$$\frac{1}{1+k_C H} = \frac{4}{5} \ \Rightarrow\ k_C = 1/(4H) = 1/(932N_0) = 0.0011\ cm/kD.$$

Estimate the parameters of Eq. (24).
By using the steady state of the Eq. (24), we have

$$\alpha_T = (\mu_T \cdot T)/C = (1.15525 \times 10^{-3}/min) \times (N_0/61N_0) = 1.89385 \times 10^{-5}/min.$$

Estimate the parameters of Eq. (25).
We consider the steady state of the Eq. (25) and obtain

$$\alpha_W = (\mu_W \cdot W)/C = (5.77623 \times 10^{-3}/min) \times (N_0/61N_0) = 9.46923 \times 10^{-5}/min.$$

References

1. Abbasi R, Marcus JM. Color pattern evolution in *Vanessa* butterflies (Nymphalidae: Nymphalini): Non-eyespot characters. Evol Dev. 2015; 17: 63-81, doi:10.1111/ede.12109.

2. Abbasi R, Marcus JM. A new A-P compartment boundary and organizer in holometabolous insect wings. Sci Rep. 2017; 7: 16337. doi:10.1038/s41598-017-16553-5.

Table 6. Molecular weights of *Bicyclus anynana* proteins. Molecular weights of *Bicyclus anynana* proteins calculated using the software www.bioinformatics.org/sms/prot-mw.html

Protein	Geneloank Acession	Protein molecular weight
Wg	XP-023955185.1	44.76 kD
Hh*	XP-023933828.1	42.32 kD
TGF-β (or dpp in *Drosophila*)	XP-023936626.1	41.07 kD

Table 7. The half-life for all components. The protein half-life for modeling degradation rates estimation.

Protein	Approximate half-life time	Species	Reference
En	30 hrs = 1800 min	cockroach	[35]
Hh (Shh protein)	50 min	Chinese hamster, human, mice	[18, 31, 56]
Ci	75 min	*Drosophila*	[4]
TGF-β (dpp in wing)	10 hrs= 600 min	*Drosophila*	[60]
Wg	2 hrs = 120 min	mouse	[73]

Table 8. The mRNA copy amounts for all components. Transcript amount for mRNA shows the proportion of protein, so this part provides relative sizes of these five components. The original experimental data is from the excel file: Özs 2017 [55] Eyespot transcripts for steady state

Protein	Relative mRNA copies amount	Species	Reference
En	185	*Bicyclus anynana*	[55]
Hh (Shh protein)	233	*Bicyclus anynana*	[55]
Ci	61	*Bicyclus anynana*	[55]
dpp	not detected (could be too small)	*Bicyclus anynana*	[55]
Wg	not detected (could be too small)	*Bicyclus anynana*	[55]

3. Allen CE, Beldade P, Zwaan BJ, Brakefield PM. Differences in the selection response of serially repeated color pattern characters: Standing variation, development, and evolution. BMC Evol Biol. 2008: 94 doi: 10.1186/1471-2148-8-94.

4. Aza-Blanc P, Ramirez-Weber FA, Laget MP, Schwartz C, Kornberg TB. Proteolysis that is inhibited by Hedgehog targets Cubitus interruptus protein to the nucleus and converts it to a repressor. Cell. 89: 1043-1053; doi: 10.1016/S0092-8674(00)80292-5.

5. Bard JBL, French V. Butterfly wing patterns: How good a determining mechanism is the simple diffusion of a single morphogen? J. Embryol. Exp. Morph. 1984; 84: 255-274.

6. Beldade P, Brakefield PM. The genetics and evo-devo of butterfly wing patterns. Nat Rev Genet. 2002; 3: 442-452.

7. Brakefield PM, French V. Butterfly wing patterns: Developmental mechanisms and evolutionary change. Acta Biotheor. 1993; 41: 447-468.

8. Brakefield PM, Gates J, Keys D, Kesbeke F, Wijngaarden PJ, Monteiro A, French V, Carroll SB. Development, plasticity and evolution of butterfly eyespot patterns. Nature. 1996; 384: 236-242.

9. Brunetti CR, Selegue JE, Monteiro A, French V, Brakefield PM, Carroll SB. The generation and diversification of butterfly eyespot colour patterns. Curr Biol. 2001; 11: 1578-1585.

10. Chang T, Mazotta J, Dumstrei K, Dumitrescu A, Hartenstein V. Dpp and Hh signaling in the Drosophila embryonic eye field. Development. 2001; 128: 4691-704. PMID: 11731450.

11. Chen Y, Goodman RH, Smolik SM. Cubitus interruptus requires Drosophila CREB-binding protein to activate wingless expression in the Drosophila embryo. Mol Cell Biol. 2000; 20: 1616-1625.

12. Chen Z, Zou Y. Anterior-posterior patterning of *Drosophila* wing discs I: A baseline mathematical model. Math Biosci. 2019; 314: 13-27.

13. Dilaõ R, Sainhas J. Modelling butterfly wing eyespot patterns. Proc. R. Soc. Lond. B. 2004; 271: 15651569.

14. Evans TM, Marcus JM. A simulation study of the genetic regulatory hierarchy for butterfly eyespot focus determination. Evol Dev. 2006; 8: 273-283.

15. Finkbeiner SD, Briscoe AD, Reed RD. Warning signals are seductive: Relative contributions of color and pattern to predator avoidance and mate attraction in *Heliconius* butterflies. Evolution. 2014; 68: 3410-3420. doi:10.1111/evo.12524, doi:10.1111/evo.12524.

16. French V, Brakefield PM. The development of eyespot patterns on butterfly wings: morphogen sources or sinks? Development. 1992; 116: 103-109.

17. French V, Brakefield PM. Eyespot development on butterfly wings: The focal signal. Dev Biol. 1995; 168: 112-123.

18. Guy RG. Inhibition of sonic hedgehog autoprocessing in cultured mammalian cells by sterol deprivation. PNAS. 2000; 97: 73077312. doi: 10.1073/pnas.97.13.7307.

19. Hannezo E, Heisenberg C-P. Mechanochemical feedback loops in development and disease. Cell. 2019; 178: 12-25.

20. Hepker J, Wang QT, Motzny CK, Holmgren R, Orenic TV. Drosophila cubitus interruptus forms a negative feedback loop with patched and regulates expression of Hedgehog target genes. Development. 1997; 124: 549-558.

21. Hill RI, Vaca JF. Differential wing strength in *Pierella* butterflies (Nymphalidae, Satyrinae) supports the deflection hypothesis. Biotropica. 2004; 36: 362-370.

22. Hiscock TW, Megason SG. Mathematically guided approaches to distinguish models of periodic patterning. Development. 2015: 142: 409-419.

23. Keys DN, Lewis DL, Selegue JE, Pearson BJ, Goodrich LV, Johnson RJ, Gates J, Scott MP, Carroll SB. Recruitment of a hedgehog regulatory circuit in butterfly eyespot evolution. Science. 1999; 283: 532-534.

24. Kingsolver JG. Thermoregulation, flight, and the evolution of wing pattern in Pierid butterflies: The topography of adaptive landscapes. Am. Zoologist. 1988; 28: 899-912.

25. Kleinschmit A, Takemura M, Dejima K, Choi PY, Nakato H. Drosophila heparan sulfate 6-O-endosulfatase Sulf1 facilitates wingless (Wg) protein degradation. J Biol Chem. 2013; 288: 5081-5089. doi:10.1074/jbc.M112.447029.

26. Koch PB, Keys DN, Rocheleau T, Aronstein K, Blackburn M, Carroll SB, et al. Regulation of dopa decarboxyklase expression during colour pattern formation in wild-type and melanic tiger swallowtail butterflies. Development 1998; 125: 23032313.

27. Koch PB, Merk R, Reinhardt R, Webe P. Localization of ecdysone receptor protein during colour pattern formation in wings of the butterfly Precis coenia (Lepidoptera : Nymphalidae) and co-expression with Distal-less protein. Dev Genes Evol. 2003; 212: 571-584.

28. Koch PB, Nijhout HF. The role of wing veins in colour pattern development in the butterfly *Papilio xuthus* (Lepidoptera: Papilionidae). Eur. J. Entomol. 2002; 99: 6272.

29. Lawrence PA, Sanson B, Vincent JP. Compartments, wingless and engrailed: patterning the ventral epidermis of Drosophila embryos. Development. 1996; 122: 4095-4103.

30. Li X, Fan D, Zhang W, Liu G, Zhang L, Zhao L, Fang X, Chen L, Dong Y, Chen Y, et al. Outbred genome sequencing and CRISPR/Cas9 gene editing in butterflies. Nature Comm. 2015; 6: 8212.

31. Mackie AR, Klyachko E, Thorne T, Schultz KM, Millay M, Ito A, Kamide CE, Liu T, Gupta R, Sahoo S, Misener S, Kishore R, Losordo DW. Sonic HedgehogModified Human CD34+ Cells Preserve Cardiac Function After Acute Myocardial Infarction. Circ Res. 2012; 111: 312-321. doi: 10.1161/CIRCRESAHA.112.266015.

32. Madzvamuse A, Maini PK, Wathen AJ, Sekimura T. A predictive model for color pattern formation in the butterfly wing of Papilio dardanus. Hiroshima Math. J. 2002; 32: 325-336.

33. Marcus JM. Evo-Devo of Butterfly Wing Patterns. Evolutionary Developmental Biology-A Reference Guide. Springer, Cham, Switzerland. 2019.

34. Marcus JM, Evans TM. A simulation study of mutations in the genetic regulatory hierarchy for butterfly eyespot focus determination. BioSystems. 2008; 93: 250-255 doi:doi:10.1016/j.biosystems.2008.05.006.

35. Marie B, Cruz-Orengo L, Blagburn JM. Persistent engrailed expression is required to determine sensory axon trajectory, branching, and target choice. J. Neurosci. 2002; 22: 832-841. doi: 10.1523/JNEUROSCI.22-03-00832.2002.

36. Marino S, Hogue IB, Ray CJ, Kirschner DE. A methodology for performing global uncertainly and sensitivity analysis in systems biology. J Theor. Biol. 2008; 254: 178-196.

37. Mercker M, Hartmann D, Marciniak-Czochra A. A mechanochemical model for embryonic pattern formation: coupling tissue mechanics and morphogen expression. PLoS One. 2013; 8: e82617.

38. Michel M, Dahmann C. Regulating mechanical tension at compartment boundaries in Drosophila. Fly (Austin). 2016; 10: 204-209. doi:10.1080/19336934.2016.1207028.

39. Monteiro A. Origin, development, and evolution of butterfly eyespots. Annu. Rev. Entomol. 2015; 60: 253-271, doi:10.1146/annurev-ento-010814-020942.

40. Monteiro A, Chen B, Ramos DM, Oliver JC, Tong XL, Guo M, Wang WK, Fazzino L, Kamal F. Distal-Less regulates eyespot patterns and melanization in bicyclus butterflies. J Exp Zool B Mol Dev Evol. 2013; 320B: 321-331 DOI: 10.1002/jez.b.22503.

41. Monteiro A, Glaser G, Stockslager S, Glansdorp N, Ramos D. Comparative insights into questions of lepidopetran wing pattern homology. BMC Dev Biol. 2006; 6: 52.

42. Mortzfeld BM, Taubenheim J, Klimovich AV, et al. Temperature and insulin signaling regulate body size in Hydra by the Wnt and TGF-beta pathways. Nat Commun. 2019; 10: 3257. https://doi.org/10.1038/s41467-019-11136-6.

43. Murray JD. On pattern formation mechanisms for lepidopteran wing patterns and mammalian coat markings. Phil Trans R Soc B. 1981; 295: 473-496.

44. Nijhout HF. Wing pattern formation in Lepidoptera: A model. J Exp Zool. 1978; 206: 119-136.

45. Nijhout HF. Pattern formation in lepidopteran wings: determination of an eyespot. Devl Biol. 1980; 80: 267-274.

46. Nijhout HF. A comprehensive model for color pattern formation in butterflies. Proc R Soc B. 1990; 239: 81-113.

47. Nijhout HF. The development and evolution of butterfly wing patterns. Smithonian Institution Press. Washington and London. 1991.

48. Nijhout HF. Genes on the wing. Science. 1994; 265: 44-45.

49. Nijhout HF. Focus on butterfly eyespot development. Nature. 1996; 384: 209-210.

50. Nijhout HF, Maini PK, Madzvamuse A, Wathen AJ, Sekimura T. Pigmentation pattern formation in butterflies: experiments and models. C. R. Biol. 2003; 326: 717-727.

51. Oppenheimer DI, MacNicol AM, Patel NH. Functional conservation of the wingless-engrailed interaction as shown by a widely applicable baculovirus misexpression system. Current Biology. 1999; 9: 1288-1296.

52. Otaki JM. Color-pattern analysis of eyespots in butterfly wings: a critical examination of morphogen gradient models. Zool Sci. 2011; 28: 403-413.

53. Otaki JM. Generation of butterfly wing eyespot patterns: a model for morphological determination of eyespot and parafocal element. Zool Sci. 2011; 28: 817-827.

54. Otaki JM. Structural analysis of eyespots: dynamics of morphogenic signals that govern elemental positions in butterfly wings. BMC Syst Biol. 2012; 6: 17.

55. Özsu N, Chan QY, Chen B, Das Gupta M, Monteiro A. Wingless is a positive regulator of eyespot color patterns in *Bicyclus anynana* butterflies. Dev Biol. 2017; 429: 177-185.

56. Pepinsky RB, Shapiro RI, Wang S, Chakraborty A, Gill A, Lepage DJ, Wen D, Rayhorn P, Horan GSB, Taylor FR, Garber EA, Galdes A, Engber TM. Long-acting forms of Sonic hedgehog with improved pharmacokinetic and pharmacodynamic properties are efficacious in a nerve injury model. J Pharm Sci. 2002; 91: 371-387. doi: 10.1002/jps.10052.

57. Platt AP, Brower LP. Mimetic versus disruptive coloration in intergrading populations of *Limenitis arthemis* and *astyanax* butterflies. Evolution. 1968; 22: 699-718.

58. Prudic KL, Timmermann BN, Papaj DR, Ritland DB, Oliver JC. Mimicry in viceroy butterflies is dependent on abundance of the model queen butterfly. Commun Biol. 2019; 2: 68, doi:10.1038/s42003-019-0303-z.

59. Robertson KA, Monteiro A. Female Bicyclus anynana butterflies choose males on the basis of their dorsal UV-reflective eyespot pupils. Proc R Soc Lond B. 2005; 272: 1541-1546.

60. Sánchez-Aragón M, Aguilar-Hidalgo D, Lehtinen B, Casares F, Iber D. A model of the spatio-temporal dynamics of Drosophila eye disc development. PLoS Comput. Biol. 2016; 12: e1005052. doi: 10.1371/journal.pcbi.1005052.

61. Sekimura T, Madzvamuse A, Wathen AJ, Maini PK. A model for colour pattern formation in the butterfly wing of Papilio dardanus. Proc. R. Soc. Lond. B. 2000; 267: 851859.

62. Sekimura T, Maini PK, Nardi JB, Zhu M, Murray JD. Pattern formation in lepidopteron wings. Comments Theor. Biol. 1998; 5; 6987.

63. Sekimura A, Venkataraman C, Madzvamuse A. A model for selection of eyespots on butterfly wings. PLoS One. 2015; 10: e0141434.

64. Sekimura T, Zhu M, Cook J, Maini PK, Murray JD. Pattern formation of scale cells in lepidoptera by differential origindependent cell adhesion. Bull. Math. Biol. 1999; 61: 807827.

65. Suzuki TK, Tomita S, Sezutsu H. Multicomponent structures in camouflage and mimicry in butterfly wing patterns. J Morphology. 2019; 280: 149-166, doi:10.1002/jmor.20927.

66. Turing AM. The chemical basis of morphogenesis. Phil. Trans. R. Soc. Lond. B. 1952; 237: 37-72.

67. Wang QT, Holmgren RA. Nuclear import of Cubitus interruptus is regulated by Hedgehog via a mechanism distinct from Ci stabilization and Ci activation. Development. 2000; 127: 3131-3139.

68. Wilts BD, Pirih P, Arikawa K, Stavenga DG. Shiny wing scales cause spec(tac)ular camouflage of the angled sunbeam butterfly, *Curetis acuta*. Biol J Linn Soc. 2013; 109: 279-289.

69. Wolpert L. Positional information and the spatial pattern of cellular differentiation. J. Theor. Biol. 1969; 25: 1-47.

70. Wolpert L. Positional information and pattern formation. Curr. Top. Dev. Biol. 1971; 6: 183-224.

71. Zhang L, Mazo-Vargas A, Reed RD. Single master regulatory gene coordinates the evolution and development of butterfly color and iridescence. PNAS. 2017; 114: 10707.

72. Zhao J, Kong Y, Zhang F, Linhardt RJ. Impact of temperature on heparin and protein interactions. Biochem Physiol. 2018; 7: 241. doi:10.4172/2168-9652.1000241.

73. Anonymous. New Wnt products added to range. Scientist Live. 2018; https://www.scientistlive.com/content/new-wnt-products-added-range.